THE MAJOR AND MINOR GALAXY MERGER RATES AT $Z < 1.5$

Jennifer M. Lotz[1,2,3], Patrik Jonsson[4], T.J. Cox[5,6], Darren Croton[7],
Joel R. Primack[8], Rachel S. Somerville[3,9], and Kyle Stewart[10,11]
accepted to the Astrophysical Journal 10 August 2011

ABSTRACT

Calculating the galaxy merger rate requires both a census of galaxies identified as merger candidates, and a cosmologically-averaged 'observability' timescale $\langle T_{obs}(z) \rangle$ for identifying galaxy mergers. While many have counted galaxy mergers using a variety of techniques, $\langle T_{obs}(z) \rangle$ for these techniques have been poorly constrained. We address this problem by calibrating three merger rate estimators with a suite of hydrodynamic merger simulations and three galaxy formation models. We estimate $\langle T_{obs}(z) \rangle$ for (1) close galaxy pairs with a range of projected separations, (2) the morphology indicator $G - M_{20}$, and (3) the morphology indicator asymmetry A. Then we apply these timescales to the observed merger fractions at $z < 1.5$ from the recent literature. When our physically-motivated timescales are adopted, the observed galaxy merger rates become largely consistent. The remaining differences between the galaxy merger rates are explained by the differences in the range of mass-ratio measured by different techniques and differing parent galaxy selection. The major merger rate per unit co-moving volume for samples selected with constant number density evolves much more strongly with redshift ($\propto (1 + z)^{+3.0 \pm 1.1}$) than samples selected with constant stellar mass or passively evolving luminosity ($\propto (1 + z)^{+0.1 \pm 0.4}$). We calculate the minor merger rate ($1:4 < M_{sat}/M_{primary} \lesssim 1:10$) by subtracting the major merger rate from close pairs from the 'total' merger rate determined by $G - M_{20}$. The implied minor merger rate is ~ 3 times the major merger rate at $z \sim 0.7$, and shows little evolution with redshift.

Subject headings: galaxies:evolution – galaxies:high-redshift – galaxies:interacting – galaxies:structure

1. INTRODUCTION

The galaxy merger rate over cosmic time is one of the fundamental measures of the evolution of galaxies. Galaxies and the dark matter halos they live in must grow with time through mergers with other galaxies and through the accretion of gas and dark matter from the cosmic web. Over the past 10 billion years, the global star-formation rate density has declined by a factor of 10 (e.g. Lilly et al. 1996; Madau et al. 1996; Hopkins & Beacom 2006) while the global stellar-mass density has increased by a factor of two (e.g. Rudnick et al. 2003; Dickinson et al. 2003) . At the same time, massive galaxies have been transformed from rapidly star-forming disk galaxies into quiescent bulge-dominated galaxies hosting super-massive black holes (e.g. Bell et al. 2004; Faber et al. 2007; Brown et al. 2007). Galaxy mergers may be an important process that drives galaxy assembly, rapid star-formation at early times, the accretion of gas onto central super-massive black holes, and the formation of dispersion-dominated spheroids (e.g. Toomre 1977; White & Rees 1978; Kauffmann, White, & Guiderdoni 1993; Mihos & Hernquist 1996; Sanders & Mirabel 1996; Somerville et al. 2001, 2008; di Matteo et al. 2008; Hopkins et al. 2006, 2008). Because other physical processes are also at work, direct observations of the galaxy mergers are needed to understand their global importance to galaxy evolution and assembly.

In a cold-dark matter dominated universe, massive structures are expected to grow hierarchically. Numerical simulations consistently predict that the dark matter halo - halo merger rate per progenitor (or descendant) halo at fixed halo mass changes rapidly with redshift $\sim (1 + z)^{2-3}$ (e.g. Gottlöber, Klypin, & Kratsvov 2001; Fakhouri & Ma 2008; Genel et al. 2009; Fakhouri, Ma, & Boylan-Kolchin 2010). The dark matter merger rate scales with mass and mass ratio (Fakhouri & Ma 2008; Fakhouri et al. 2010). More massive halos are rarer, but have more frequent merger rates per halo. Minor mergers with mass ratios greater than 1:4 should be much more common per halo than major mergers with comparable mass halos.

However, the theoretical predictions for the *galaxy* merger rate remain highly uncertain (e.g. Jogee et al. 2009; see Hopkins et al. 2010a for a review). The predicted $(1 + z)^3$ evolution in the dark-matter halo merger rate (per halo above a fixed total mass) does not automatically translate into a $(1 + z)^3$ evolution in the galaxy merger rate (per galaxy above a fixed stellar mass) because there is not a simple connection between observed galaxies and dark matter halos (e.g. Berrier et al. 2006; Hopkins et al. 2010a, Moster et al. 2010). For example, the differences in the dark matter halo mass function

[1] National Optical Astronomical Observatories, 950 N. Cherry Avenue, Tucson, AZ 85719, USA
[2] Leo Goldberg Fellow
[3] Space Telescope Science Institute, 3700 San Martin Dr., Baltimore, MD 21218; lotz@stsci.edu
[4] Harvard-Smithsonian Center for Astrophysics, Cambridge, MA, USA
[5] Carnegie Observatories, Pasadena, CA, USA
[6] Carnegie Fellow
[7] Centre for Astrophysics & Supercomputing, Swinburne University of Technology, Hawthorn, Australia
[8] Department of Physics, University of California, Santa Cruz, USA
[9] Department of Physics & Astronomy, Johns Hopkins University, Baltimore, MD, USA
[10] Jet Propulsion Laboratory, Pasadena, CA, USA
[11] NASA Postdoctoral Fellow

and the galaxy stellar mass function at the high mass and low mass ends naturally produces a discrepancy between the merger rates as a function of stellar and dark-matter mass and mass ratio.

Many galaxy evolution models predict that the evolution of major mergers of galaxies selected above a fixed stellar mass ($\sim 10^{10} M_\odot$) changes more modestly with redshift ($\sim (1+z)^{1-2}$), but these can have an order of magnitude variation in their normalizations (e.g. Jogee et al. 2009; Hopkins et al. 2010a). The largest source of theoretical uncertainty for semi-analytic galaxy evolution models is the baryonic physics required to map galaxies onto dark matter halos and sub-halos, and in turn, required to match the observational selection of luminous merging galaxies (Hopkins et al. 2010a and references therein). In contrast, semi-empirical models which map galaxies onto dark matter sub-halos by matching the observed abundances of galaxies (per unit luminosity) to the abundances of sub-halos (per unit mass) give reasonably good predictions for clustering statistics by adopting fairly small dispersions in the mapping function (e.g. Zheng et al. 2007, Conroy & Wechsler 2009) and give a only factor of two discrepancy in the predicted major merger rates (e.g. Hopkins et al. 2010b, Stewart et al. 2009a).

Despite more than a decade of work, measurements of the observed galaxy merger rate and its evolution with redshift has not converged. Current observations of the fraction of bright/massive galaxies undergoing a merger differ by an order of magnitude (Fig. 1), and estimates of the evolution in this merger fraction of at $0 < z < 1.5$ vary from weak or no evolution (e.g. Bundy et al. 2004; Lin et al 2004; Lotz et al. 2008a; Jogee et al. 2009; Bundy et al. 2009; Shi et al. 2009; de Ravel et al. 2009; Robaina et al 2010) to strong evolution ($\sim (1+z)^3$; Le Feýre et al. 2000; Conselice et al. 2009; Cassata et al. 2004; Kartaltepe et al. 2007; Rawat et al. 2008; Bridge et al. 2010; López-Sanjuan et al. 2009). It has been difficult to understand the source of these discrepancies, as the various studies often employ different criteria for counting galaxy mergers and different selections for the parent galaxy samples.

These observational studies identify galaxy merger candidates either as galaxies in close pairs (in projected or real 3-D space) or galaxies with distorted morphologies (measured quantitatively or by visual inspection). A key obstacle to the consistent measurement of the galaxy merger rate has been the poorly constrained timescales for detecting galaxy mergers selected by different methods. Close pairs find galaxies before they merge, while merger-induced morphological disturbances can appear before, during, and after a galaxy merger. Moreover, morphological studies use a variety of tracers to classify galaxies as mergers (such as $G - M_{20}$, asymmetry, tidal tails), which have differing sensitivities to different merger properties such as mass ratio and gas fraction. Thanks to new high-resolution hydrodynamical simulations of galaxy mergers which model realistic light profiles including the effects of star-formation and dust (e.g. Jonsson et al 2006), it is now possible to estimate the timescales for detecting galaxy mergers with a variety of close pair and morphological criteria (Lotz et al. 2008b; Lotz et al. 2010a, b). These simulations also span a range of merger properties, including progenitor mass, mass ratio, gas fraction, and orbital parameters (Cox et al. 2006, 2008). Mass ratio and gas fraction are especially important for interpreting the merger fractions derived from morphological studies (Lotz et al. 2010a, b).

The goal of this paper is to self-consistently determine the observational galaxy merger rate at $z < 1.5$ from recent close pair and morphological studies. We weight the merger timescales from individual high-resolution simulations by the expected distribution of merger properties (including gas fraction and mass ratio) to determine the average observability timescale as a function of redshift for each method for finding galaxy mergers (close pairs, $G - M_{20}$, asymmetry). These new calculations of the average observability timescales are crucial for interpreting the observed galaxy merger fractions. We re-analyze the observations of galaxy mergers at $z < 1.5$ from the recent literature and derive new estimates of the galaxy merger rate. We also carefully consider the effects of parent sample selection on the inferred evolution of the galaxy merger rate. We conclude that the differences in the observed galaxy merger fractions may be accounted for by the different observability timescales, different mass-ratio sensitivities, and different parent galaxy selections. When these differences in the methodology are properly accounted for by adopting our derived timescales, we are able to derive self-consistent estimates of the major and minor galaxy merger rate and its evolution.

In §2, we define the volume-averaged galaxy merger rate, Γ_{merg}, as the co-moving number density of on-going galaxy merger events per unit time, and the fractional galaxy merger rate, $\Re_{merg}$, as the number of galaxy merger events per unit time per selected galaxy. We discuss how to calculate Γ_{merg} and $\Re_{merg}$ using close pairs and disturbed morphologies. In §3, we review the recent literature estimates of the galaxy merger fraction using quantitative morphology ($G - M_{20}$, asymmetry) and close pairs of galaxies and discuss the importance of the parent sample selection. In §4, we review the results from the individual high-resolution galaxy merger simulations. We present new calculations of the cosmologically-averaged merger observability timescale $\langle T_{obs}(z) \rangle$ for close pairs, $G - M_{20}$, and asymmetry, using the distribution of galaxy merger properties predicted by three different galaxy evolution models (Croton et al. 2006; Somerville et al. 2008; Stewart et al. 2009b). In §5, we derive the fractional and volume-averaged major and minor galaxy merger rates for galaxy samples selected by stellar-mass, evolving luminosity, and constant co-moving number density at $z < 1.5$. We compare these results to the predicted major and minor galaxy merger rates. Throughout this work, we assume $\Omega_m = 0.3$, $\Omega_\Lambda = 0.7$, and $H_0 = 70$ km s^{-1} Mpc^{-1}, except for close pair projected separations where $h = H_0/100$ km s^{-1} Mpc^{-1}.

2. CALCULATING THE GALAXY MERGER RATE

The volume-averaged galaxy merger rate Γ_{merg} is defined as the number of on-going merger events per unit co-moving volume, ϕ_{merg}, divided by the time T_{merg} for the merger to occur from the initial encounter to the final coalescence:

$$\Gamma_{merg} = \frac{\phi_{merg}}{T_{merg}} \qquad (1)$$

Note that T_{merg}, the time period between the time of the initial gravitational encounter and coalescence (from "not merging" to "merged") is not well defined.

More accurately, the number density of galaxies identified as galaxy mergers ϕ_{merg} will depend on the average timescale $\langle T_{obs} \rangle$ during which the merger can be observed given the method used to identify it, such that

$$\phi'_{merg} = \phi_{merg} \frac{\langle T_{obs} \rangle}{T_{merg}} \qquad (2)$$

A galaxy merger may be identified at discontinuous stages (as in the case of close pairs), therefore T_{obs} is the sum of the observability windows.

Thus, the galaxy merger rate Γ can be calculated from the observed number density of galaxy merger candidates ϕ'_{merg} as follows:

$$\Gamma_{merg} = \frac{\phi'_{merg}}{T_{merg}} \frac{T_{merg}}{\langle T_{obs} \rangle} = \frac{\phi'_{merg}}{\langle T_{obs} \rangle} \qquad (3)$$

The majority of past merger calculations have assumed $\langle T_{obs} \rangle$ to be a constant value ranging from ~ 0.2 Gyr to 1 Gyr, without considering the differences in methodology, the effect of merger parameters, or redshift-dependent changes in the ability to detect mergers. In §4, we present detailed calculations of $\langle T_{obs} \rangle$ as a function of redshift for different methods using theoretical models of galaxy interactions and the evolving distribution of galaxy merger properties.

Galaxy mergers can be directly identified as close galaxy pairs that have a high probability of merging within a short time. Galaxies with similar masses that lie within a hundred kpc of each other and have relative velocities less than a few hundred km s^{-1} are likely to merge within a few billion years. Individual close galaxy pairs may be found by counting up the numbers of galaxies with companions within a given projected separation R_{proj} and within a relative velocity or redshift range. However, spectroscopic determination of the relative velocities of close pairs is observationally expensive, and prone to incompleteness due to slit/fiber collisions and biased detection of emission-line galaxies (e.g. Lin et al. 2004, 2008; de Ravel et al. 2009). Photometric redshifts are often used as a proxy for spectroscopic velocity separations (e.g. Kartaltepe et al. 2007, Bundy et al. 2009). However, even high precision photometric redshifts ($\frac{\delta z}{1+z} \sim 0.02$) are only accurate to 100-200 Mpc along the line of sight. Therefore significant statistical corrections for false pairs are required for photometrically selected pair studies (e.g. Kartaltepe et al. 2007). Finally, two-point angular correlation studies of large samples of galaxies have also been used to determine the statistical excess of galaxies within a given dark matter halo (e.g. Masjedi et al. 2006, Robaina et al. 2010). These studies are less prone to line-of-sight projection issues, but cannot identify individual merging systems.

Morphological disturbances also indicate a recent or on-going merger. Galaxy mergers experience strong gravitational tides, triggered star-formation, and the redistribution of their stars and gas into a single relaxed galaxy. This gravitational rearrangement results in morphological distortions – e.g. asymmetries, double nuclei, tidal tails – which are detectable in high-resolution images. Such disturbances can be found through visual inspection by human classifiers, or by quantitative measurements of galaxy structures. Several different quantitative methods are commonly used to measure galaxy morphology and classify galaxy mergers. Rotational asymmetry (A) picks out large-scale high surface brightness asymmetric structures (e.g. Abraham et al. 1994; Conselice, Bershady, & Jangren 2000; Conselice 2003); the combination of the Gini coefficient (G; Abraham et al. 2003; Lotz et al. 2004) and second-order moment of the brightest 20% of the light (M_{20}) selects galaxies with multiple bright nuclei (Lotz et al. 2004). Both of these methods require high signal-to-noise and high spatial resolution images generally only achievable with the Hubble Space Telescope (HST) at $z > 0.3$, as well as a training set to distinguish 'normal' galaxies from merger candidates.

The merger fraction, f_{merg}, is the fraction of galaxies identified as mergers for a given galaxy sample, and is often presented instead of the number density of observed merger events. Thus ϕ'_{merg} depends on both the merger fraction and the co-moving number density of galaxies in the selected sample, n_{gal}:

$$\phi'_{merg} = f_{merg} n_{gal} \qquad (4)$$

For both morphologically-selected and close pair merger candidates, a correction factor is applied to the merger fraction to account for contamination from objects that are not mergers. For morphological merger selection, this correction is applied prior to calculating f_{merg} based on visual inspection or a statistical correction. For close pairs, the fraction of pairs (f_{pair}) or the fraction of galaxies in a pair ($N_c \sim 2 f_{pair}$) is multiplied by this correction factor C_{merg}, such that

$$f_{merg} = C_{merg} f_{pair} \sim C_{merg} \frac{N_c}{2} \qquad (5)$$

We will adopt $C_{merg} = 0.6$ throughout this paper. Numerical simulations and empirical measurements suggest that C_{merg} is $\sim 0.4-1.0$ for close pairs selected with projected separations $< 20-30$ kpc h^{-1} (Kitzbichler & White 2008, Patton & Atfield 2008; see Bundy et al. 2009 for discussion). It is worth noting that close pair samples are likely to be biased towards objects in groups or clusters (Barton et al. 2007), although simulations suggest that the majority of these objects will merge (Kitzbichler & White 2008).

Multiple authors have estimated the fractional merger rate $\Re_{merg}$ instead of Γ_{merg} where

$$\Re_{merg} = \frac{f_{merg}}{\langle T_{obs} \rangle} = \frac{C_{merg} f_{pair}}{\langle T_{obs} \rangle} \qquad (6)$$

(e.g. López-Sanjuan et al. 2009, Bundy et al. 2009, Bridge, Carlberg, & Sullivan 2010, Conselice et al. 2009, Jogee et al. 2009). In principle, the fractional merger rate $\Re_{merg}$ circumvents variation in n_{gal}, which may change from field to field with cosmic variance and is a factor of two or more lower at $z \sim 1$ than $z \sim 0.2$ for fixed stellar mass or passive luminosity evolution selection (Figure 2). Semi-analytic cosmological simulations also have difficulty simultaneously reproducing the correct galaxy number densities at all mass scales, but may

be more robustly compared to observations for relative trends such as $\Re_{merg}$.

Γ_{merg} traces the number of merger events per comoving volume above some mass/luminosity limit, while $\Re_{merg}$ traces the number of merger events per (bright/massive) galaxy. It is often implicitly assumed that any evolution with redshift is not dependent on $n_{gal}(z)$ or the galaxy selection either because the parent galaxy samples are selected in a uniform way or because the merger rate is not a strong function of galaxy luminosity, mass, or number-density. However, several studies have found that the fraction of mergers increases significantly at fainter absolute magnitudes/lower stellar masses (Bridge et al. 2010; de Ravel et al. 2009; Lin et al. 2004; Bundy et al 2005), while other studies have found increased merger fractions for more massive galaxies (Bundy et al. 2009; Conselice et al. 2003). If the observed merger fraction depends upon luminosity or stellar mass, comparison of different observational estimates of Γ_{merg} or $\Re_{merg}$ will require careful consideration of the parent galaxy sample selection criteria. We will return to this issue in §3.5.

3. GALAXY MERGER OBSERVATIONS

Despite the large number of galaxy merger studies, there is little consensus on the galaxy merger rate or its evolution with redshift at $z < 1.5$. In part, this is because many studies have compared the galaxy merger fraction $f_{merg}(z)$ (Figure 1) or the galaxy merger rate for galaxy merger samples selected with different approaches and/or with different parent sample criteria. In this section, we review the selection of galaxy mergers and their parent samples for a variety of recent merger studies at $z < 1.5$. We will focus on works that identify merger via quantitative morphology ($G - M_{20}$, A) or close pairs, but briefly discuss results from other approaches. Almost all of these studies have calculated either the evolution in the merger fraction (f_{merg} or f_{pair}), thereby ignoring $\langle T_{obs}(z) \rangle$, or the merger rate Γ_{merg} or $\Re_{merg}$ by assuming a constant $\langle T_{obs} \rangle$ with redshift.

3.1. $G - M_{20}$-Selected Mergers

One quantitative morphological approach to identifying galaxy mergers in high-resolution images has been the $G - M_{20}$ method. The Gini coefficient G is a measurement of the relative distribution of flux values in the pixels associated with a galaxy, such that uniform surface brightness galaxies have low G and galaxies with very bright nuclei have high G (Abraham et al. 2003; Lotz et al. 2004). When G is combined with M_{20}, the second-order moment of the brightest 20% of the light, local spiral and elliptical galaxies follow a well-defined sequence and local mergers have higher G and and higher M_{20} values (Lotz et al. 2004). Simulations of galaxy mergers revealed that the $G - M_{20}$ technique primarily identifies mergers during the first pass and final merger (Lotz et al. 2008b) and is sensitive to mergers with baryonic mass ratios between 1:1 - 1:10 (Lotz et al. 2010b). It has been noted by multiple authors that the merger sample found by the $G - M_{20}$ technique is incomplete (Kampczyk et al. 2007; Scarlata et al. 2007; Kartaltepe et al. 2010). This is consistent with the results from galaxy merger simulations, which predict that $G - M_{20}$

identifies merging systems for only a short period while double nuclei are evident (Lotz et al. 2008; Lotz et al. 2010a, b).

By applying the $G - M_{20}$ technique to high-resolution HST Advanced Camera for Surveys V (F606W) and I (F814W) images of the Extended Groth Strip (Davis et al. 2007), Lotz et al. (2008a) found $f_{merg} = 10 \pm 2\%$ for a sample of galaxies at $0.2 < z < 1.2$. This work concluded that the galaxy merger fraction and rate evolved weakly over this redshift range: $f_{merg}(z) \propto (1 + z)^{0.23 \pm 1.03}$. The parent sample was selected to be brighter than $0.4 L_B^*(z)$, assuming passive luminosity evolution of galaxies and rest-frame B luminosity functions calculated for the Extended Groth Strip ($M_B < -18.94 - 1.3z$; Faber et al. 2007). Only rest-frame B morphologies were considered in order to avoid biases associated with intrinsic morphological dependence on rest-frame wavelength. The merger fractions were corrected for visually- and spectroscopically-identified false mergers ($\sim 20-30\%$ of initial merger candidates, similar to photometric redshift pair corrections). $G - M_{20}$ identified merger candidates with visually-identified artifacts or foreground stars were removed from the sample. Also, $G - M_{20}$ merger candidates with multiple spectroscopic redshifts within a single DEEP2/DEIMOS slit were identified and used to statistically correct the resulting merger fractions (see Lotz et al. 2008a for additional discussion.) The statistical uncertainties associated with galaxies scattering from the main locus on normal galaxies to merger-like $G-M_{20}$ values are also included in the merger fraction error. The f_{merg} and n_{gal} values from Lotz et al. (2008a) are given in Table 2.

For this paper, we have also computed $f_{merg}(G-M_{20})$ for a parent sample selected above a fixed stellar mass $M_{star} > 10^{10} M_\odot$ for the same HST observations of the Extended Groth Strip. (Stellar masses were calculated using Bruzual & Charlot 2003 spectral energy distributions and a Chabrier 2003 initial mass function; see Salim et al. 2009, 2007 for details). We estimated n_{gal} using the galaxy stellar mass functions v. redshift given by Ilbert et al. (2010) for the same redshift bins. We note that these were derived using a different field (COSMOS), but are consistent with the galaxy stellar mass function computed for the Extended Groth Strip with larger redshift bins (Bundy et al. 2006).

3.2. Asymmetric Galaxies

Another commonly-used measure of morphological disturbance is the rotational asymmetry, A. Asymmetry measures the strength of residuals when a galaxys profile is subtracted from its 180-degree rotated profile (Abraham et al. 1994; Conselice et al. 2000). Merger simulations suggest that high A values may last for a longer period of time than $G-M_{20}$ detected disturbances (Lotz et al. 2008b, 2010a,b). As we discuss in §4, A is highly sensitive to gas fraction and, for local gas fractions, probes mergers with a different range of mass ratio than $G-M_{20}$.

Early studies of small deep HST fields by Abraham et al. (1996) and Conselice et al. (2003, 2005) showed strong evolution in the fraction of asymmetric galaxies at $0 < z < 3$ with stellar masses $> 10^{10} M_\odot$. Subsequent studies based on larger HST surveys confirmed this initial result at $0 < z < 1.2$ (Cassata et al. 2005, Conselice et al. 2009, López- Sanjuan et al. 2009; but see Shi et
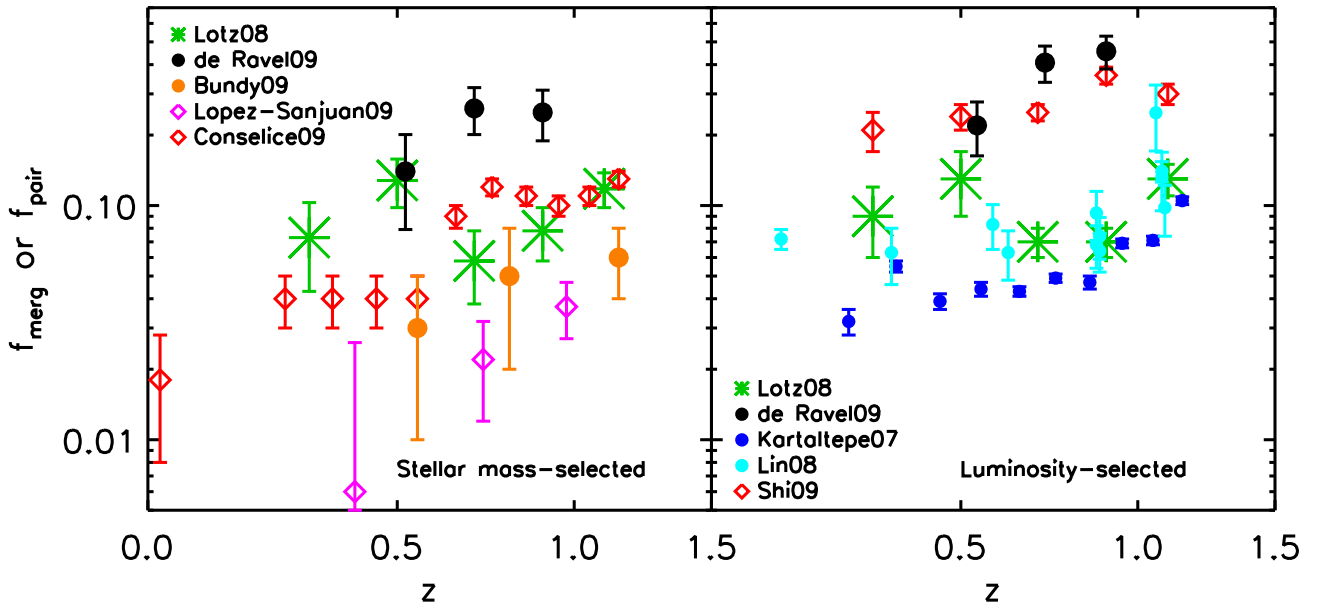
FIG. 1.— Left: The galaxy merger fraction (f_{merg}) or close pair fraction (f_{pair}) v. redshift for samples selected by stellar mass ($M_{star} > 10^{10} M_\odot$). Right: Same, for samples selected with an evolving luminosity limit (see text). Large asterisks are $G - M_{20}$-selected mergers, filled circles are for close pairs, and open diamonds are for asymmetric galaxies. For both stellar-mass and luminosity-selected parent samples, f_{merg} and f_{pair} vary by a factor of 10 for different merger studies.

al. 2009). For this paper, we consider the measurements for three recent studies: Conselice et al. (2009), López-Sanjuan et al. (2009) and Shi et al. (2009). These studies compute A in rest-frame B. Low signal-to-noise images and redshift-dependent surface-brightness dimming can produce strong biases in the asymmetry measurements. Each of these asymmetry studies makes different assumptions about how to correct for these effects, and it is therefore perhaps not surprising that they draw different conclusions about $f_{merg}(z)$.

Conselice et al. (2009) computed asymmetry fractions for galaxies at $0.2 < z < 1.2$ selected from the COSMOS (Scoville et al. 2007), GEMS (Rix et al. 2004), GOODS (Giavalisco et al. 2004) and AEGIS (Davis et al. 2007) HST surveys. They find that the fraction of galaxies with stellar masses $> 10^{10} M_\odot$ that have high asymmetry increases from $\sim 4\%$ at $z = 0.2$ to 14% at $z = 1.2$, with $f_{merg}(z) \propto (1+z)^{2.3\pm0.4}$. These asymmetry fractions are corrected for an assumed mean decrease in asymmetry with redshift due to surface-brightness dimming ($\langle \delta A \rangle = -0.05$ at $z = 1$). False merger candidates scattered to high A values are visually identified and removed from the final asymmetric galaxy fractions, as are galaxies with high A but low clumpiness (S) values.

López-Sanjuan et al. (2009) also compute the fraction of asymmetric galaxies in the GOODS fields selected from a parent sample at $z < 1$ with stellar masses $> 10^{10} M_\odot$. They find even stronger evolution in the merger fraction $f_{merg}(z) \propto (1 + z)^{5.4\pm0.4}$. They apply a similar redshift-dependent correction for surface-brightness dimming to the measured asymmetry values, but correct their asymmetry values to the values expected to be observed at $z = 1$, rather than $z = 0$ as Conselice et al. 2009 does. This results in lower f_{merg}

values. Also, rather than visually inspecting the asymmetric merger candidates for false mergers, they employ a maximum-likelihood approach to determine how many normal galaxies are likely to be scattered to high asymmetry values via large measurement errors and infer a high contamination rate ($> 50\%$). Consequently, their merger fractions are much lower than Conselice et al. (2009), but follow similar evolutionary trends with redshift.

Shi et al. (2009) also examine the fraction of asymmetric galaxies in HST images of the GOODS fields. However, they select galaxies based on an evolving luminosity cut ($M_B < -18.94 - 1.3z$) and apply different corrections for the effects of sky noise and surface-brightness dimming to the asymmetry measurements. Shi et al. (2009) find that the fraction of asymmetric galaxies has not evolved strongly at $z < 1$ with $f_{merg}(z) \propto (1+z)^{0.9\pm0.3}$, but find asymmetric fractions $2 - 3$ times higher than Conselice et al. (2009). Shi et al. (2009) note that in addition to a redshift-dependent surface-brightness dimming correction to the measured asymmetry values, correction based on the signal-to-noise of the image may be required. Extremely deep images (i.e. the Hubble Ultra Deep Field; Beckwith et al. 2006) can give asymmetry values $0.05 - 0.10$ higher than lower signal-to-noise images of the same galaxy (Shi et al. 2009; Lotz et al. 2006). Based on extensive simulations of this effect, Shi et al. (2009) correct the observed fractions of asymmetric galaxies to that expected for high signal-to-noise observations in the local universe. No correction for falsely-identified merger candidates is applied, hence the Shi et al. (2009) results may be considered an upper limit to the fraction of asymmetric galaxies while the López-Sanjuan et al. (2009) result may be considered a lower limit. It

is also possible that the different signal-to-noise thresholds for detecting asymmetry probe different processes (clumpy star-formation, minor mergers, major mergers).

3.3. Close Pairs

Numerous studies have attempted to measure the galaxy merger rate by counting the numbers of galaxies with close companions. However, these studies often adopt different criteria for the projected separation of galaxies, the stellar mass (or luminosity) ratio of primary and companion galaxy, and the stellar mass (or luminosity) range of the parent sample. We can account for different projected separation criteria in our estimates of the merger rate by modifying the dynamical timescale. But without a priori knowledge of how the merger rate depends on mass ratio and mass, we cannot compare merger studies where close pairs are selected with different mass ratios or from samples with different limiting masses. Here we describe the different criteria adopted by different studies, and how these criteria are likely to affect our derivation of the merger rate. We divide these studies into those selected by stellar mass and those selected by rest-frame luminosities. We calculate $\langle T_{obs}(z) \rangle$ for each of the close pair selection criteria in §4, and assume $C_{merg} = 0.6$ for all samples when calculating the merger rates in §5.

3.3.1. Luminosity-selected pairs

Lin et al. (2008) find weak evolution in the pair fraction between $0 < z < 1.1$, with $f_{pair} \propto (1 + z)^{0.4 \pm 0.2}$. This work reanalyzes paired galaxies from the Team Keck Treasury Redshift Survey (Wirth et al. 2004), DEEP2 Galaxy Redshift Survey (Davis et al. 2004; Lin et al. 2004), CNOC2 Survey (Yee et al. 2000; Patton et al. 2002), and Millennium Galaxy Survey (Liske et al. 2003; de Propris et al. 2005) with a uniform selection criteria. They require that both objects in the pair have spectroscopic redshifts, relative velocities $\delta V < 500$ km s^{-1}, and projected separations $10 < R_{proj} < 30$ kpc h^{-1}. In order to restrict their sample to major mergers, they select only galaxies and their companion within a limited rest-frame B luminosity range corresponding to a luminosity ratio 1:1 - 1:4. Based on the evolution of the rest-frame B galaxy luminosity function with redshift observed by DEEP2 (Willmer et al. 2006; Faber et al. 2007), they assume that the typical galaxy fades by $1.3M_B$ per unit redshift, and therefore have a redshift-dependent luminosity range $-21 < M_B + 1.3z < -19$. An additional complication is the correction for paired galaxies where a spectroscopic redshift is not obtained for one galaxy in the pair, either because of the spectroscopic survey sampling (not observed) or incompleteness (not measurable). This correction is a function of color, magnitude, and redshift, and therefore is not trivial to compute. We give N_c (uncorrected) values and completeness-corrected pair fractions f_{pair} from Lin et al. (2008) in Table 1.

de Ravel et al. (2009) recently completed a similar study, using galaxies with spectroscopic redshifts $0.5 < z < 0.9$ from the VIRMOS VLT Deep Survey (VVDS). They find that the evolution in the pair fraction depends on the luminosity of the parent sample, with brighter pairs showing less evolution ($f_{pair} \propto (1 + z)^{1.5 \pm 0.7}$) than fainter pairs ($f_{pair} \propto (1 + z)^{4.73 \pm 2.01}$). (See also López-Sanjuan et al. 2011 for an analysis of minor mergers

with the same data.) We will examine only the bright sample results, as this selection ($M_B < -18.77 - 1.1z$) is similar to the Lin et al. (2008) study. They adopt a similar luminosity ratio for the paired galaxies (1:1 - 1:4) to the Lin et al. 2008 study. They also compute the pair fraction f_{pair} at several different projected separations. We use their values for $R_{proj} < 100$ kpc h^{-1} and $\delta V \leq 500$ km s^{-1} because these have the smallest statistical errors and give merger rates consistent with smaller projected separation. The number density of galaxies was computed using the VVDS rest-frame B luminosity functions (Ilbert et al. 2005).

Kartaltepe et al. (2007) used photometric redshifts to select objects at $0.2 < z < 1.2$ with close companions from deep K-band imaging of the COSMOS field. They find that the pair fraction evolves strongly with redshift $f_{pair} \propto (1 + z)^{3.1 \pm 0.1}$, in rough agreement with a later study by Rawat et al. (2008) of J-band selected pairs in the Chandra Deep Field South. To minimize the contamination from false pairs, they applied a stricter projected separation criteria of $5 < R_{proj} < 20$ kpc h^{-1} and $\delta z_{phot} \leq 0.05$. They also selected pairs of galaxies where both objects were brighter than a fixed absolute magnitude $M_V = -19.8$ which corresponds to L_V^* at $z = 0$. They correct the pair fractions for contamination rates for each redshift bin ($\sim 20-30\%$). The range of mass ratios is not well-defined, but $> L^*$ galaxies are rare, thus the majority of pairs will have luminosity ratios between 1:1 and 1:4.

Because their luminosity selection does not evolve with redshift, the Kartaltepe study probes a fainter parent population of galaxies at $z \sim 1$ and brighter parent population at $z \sim 0.2$ relative to the de Ravel and Lin et al. spectroscopic pair studies and the Lotz et al. (2008a) $G - M_{20}$ study. This makes it difficult to directly compare the Kartaltepe et al. (2007) results to other studies which adopt evolving luminosity selection. They do consider the evolution of f_{pair} when an evolving luminosity cut $M_V < -19.8 + 1.0z$ is adopted, and find that their conclusions about the evolution of $f_{pair}(z)$ do not change. In this work, we will use the COSMOS pair fractions selected with $M_V < -19.8 - 1.0z$ (J. Kartaltepe, private communication) to compare with the other merger studies. Because no published rest-frame V luminosity function is available for the COSMOS field, we estimate n_{gal} for $M_V < -19.8 - 1.0z$ from the Ilbert et al. (2005) rest-frame V-band luminosity function of the VVDS field. We will return to the issue of parent sample selection and its effects on the evolution in the observed galaxy merger rate in §3.5 .

Patton & Atfield (2008) select $z \sim 0.05$ close pairs with spectroscopic redshifts from the Sloan Digital Sky Survey. These are required to have $\delta V < 500$ km s^{-1}, $5 < R_{proj} < 20$ kpc h^{-1}, and rest-frame r-band luminosity ratios between 1:1 and 1:2. The parent sample is drawn from galaxies with $-22 < M_r < -18$. They derive a completeness-corrected value of $N_c = 0.021 \pm 0.001$. Patton & Atfield argue that between 50-80% of these pairs are line-of-sight projections, higher than the 40% ($C_{merg} \sim 0.6$) assumed here and in other works.

3.3.2. Stellar-mass selected pairs

In order to avoid assumptions about galaxy rest-frame luminosity evolution, Bundy et al. (2009) select galaxy pairs in the GOODS fields based on a fixed stellar mass and find that the pair fraction does not evolve strongly at $z < 1.2$, with $f_{pair} \propto (1+z)^{1.6\pm1.6}$. They compute stellar masses by fitting the galaxies' spectral energy distributions ($0.4 - 2$ μm) with Bruzual & Charlot (2003) stellar population models, assuming a Chabrier (2003) stellar initial mass function. The galaxy sample is selected above a fixed stellar mass limit of $M_{star} \geq 10^{10}M_\odot$. Close pairs are selected to be within $5 < R_{proj} < 20$ kpc h^{-1} and with stellar mass ratios between 1:1 and 1:4. Bundy et al. (2009) includes paired galaxies with both spectroscopic and photometric redshifts where $\delta z^2 < \sigma^2_{z,primary} + \sigma^2_{z,satellite}$ and the typical photometric redshift error $\sigma_z < 0.08(1 + z)$. We estimate the number density of GOODS galaxies with stellar masses $> 10^{10}M_\odot$ from Bundy et al. (2005).

In addition to their luminosity-based selection, de Ravel et al. (2009) also select spectroscopic VVDS galaxy pairs by stellar mass. The derived pair fraction evolution depends on the stellar mass limit of the sample, with more massive pairs showing weak evolution ($f_{pair} \propto (1 + z)^{2.04\pm1.65}$), consistent with the Bundy et al. (2009) results. Their stellar masses are computed with similar population synthesis models and multi-wavelength photometric data to the Bundy et al. (2009). de Ravel et al. (2009) assumes a modest evolution of stellar mass and selects a parent sample with an evolving stellar mass limit $\log[M_{star}/10^{10}M_\odot] > 0.187z$. As for the luminosity selected sample, we use de Ravel et al. 's spectroscopic pairs with $R_{proj} < 100$ kpc h^{-1} and $\delta V \leq 500$ km s^{-1}. Galaxy pairs are required to have stellar mass ratio between 1:1 and 1:4. We estimate the number density of galaxies from the Pozzetti et al. (2007) K-selected stellar mass functions computed for the VVDS.

3.4. *Visually Classified Mergers*

The visual classification of morphologically disturbed galaxies has a long history (e.g. Hubble 1926), and has increased in scale and sophistication. Several recent studies have estimated the galaxy merger fraction and rate using large samples of visually-classified mergers at $z < 1.5$, including the Galaxy Zoo project (Darg et al. 2010; also Jogee et al. 2009; Bridge et al. 2010; Kartaltepe et al. 2010). However, studies of the evolution of visually-classified mergers also reach contradictory conclusions.

Jogee et al. (2009) visually classified galaxies with stellar masses $> 2.5 \times 10^{10}M_\odot$ at $0.24 < z < 0.80$ in V-band $HST ACS$ images from the GEMS survey. They identify mergers as objects with asymmetries, shells, double nuclei, or tidal tails but exclude obvious close or interacting pairs. They find that $\sim 9\%$ of the sample were visually-disturbed with little evolution between $z \sim 0.2$ and $z \sim 0.8$. Between 1-4% of the sample are classified as major mergers and 4-8% are classified as minor mergers. They conclude that while most massive galaxies have undergone a major or minor merger over the past 7 Gyr, visually-disturbed galaxies account for only 30% of the global star-formation at those epochs.

Bridge et al. (2010) also visually identify galaxy mergers at $z < 1$, but reach fairly different conclusions. The
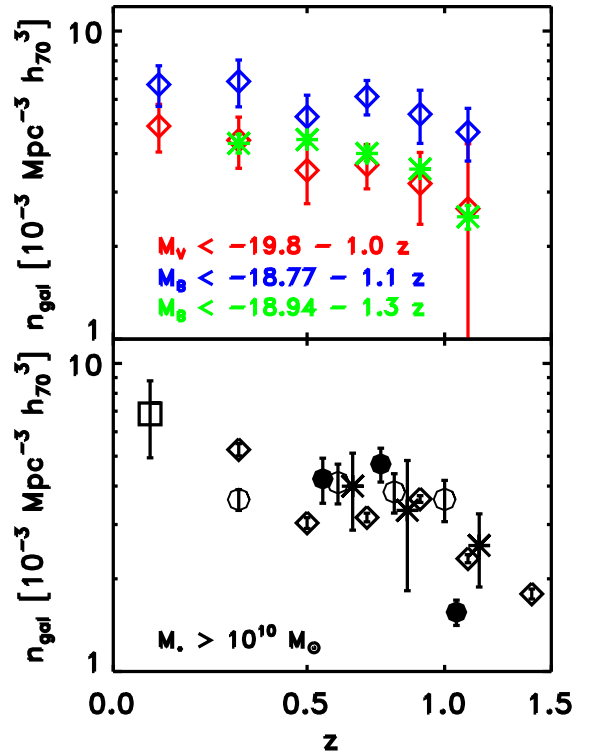

FIG. 2.— Top: Number of galaxies per co-moving unit volume n_{gal} v. redshift for the evolving luminosity selection calculated from Ilbert et al. 2005 (VVDS V-band selected, red diamonds; VVDS B-band selected blue diamonds) and Faber et al. 2007 (DEEP2 B-band selected, green asterisks); Bottom: $n_{gal}(z)$ for galaxies selected with $M_{star} > 10^{10}M_\odot$ from Bell et al. 2003 (2MASS, black square), Bundy et al. 2005 (GOODS, black filled circles), Ilbert et al. 2009 (black diamonds), Pozzetti et al. 2007 (VVDS, open circles), and Bundy et al 2006 (DEEP2, black asterisks).

Bridge et al. (2010) study is based upon very deep ground-based images from the CFHT Legacy Survey, therefore has worse spatial resolution than HST-based studies but reaches comparable limiting surface brightnesses over a much wider area. They identify merging and interacting galaxies via extended tidal tails and bridges for a sample of $\sim 27,000$ galaxies with $i < 22$ Vega mag. They find the merger fraction of galaxies with $i < 22$ and stellar mass $> 3 \times 10^9 M_\odot$ increases rapidly from $\sim 4\%$ at $z \sim 0.4$ to $\sim 19\%$ at $z \sim 1$, with an evolution $\propto (1 + z)^{2.25\pm0.24}$.

We will not attempt to incorporate these results into our study here. Visual classification of galaxy mergers is qualitative by nature, and the exact merger identification criteria applied for each study depends on the human classifiers as well as the spatial resolution and depth of the imaging data. Therefore visual classification observability timescales are unique to each study and less straightforward to calculate than for the quantitative and easily reproducible (but possibly less sensitive; Kartaltepe et al. 2010) methods that we use in this work.

3.5. *The Importance of Sample Selection*

Often the merger fraction f_{merg} is measured over a range of redshifts where the galaxy mass and luminosity functions change significantly (e.g. Faber et al. 2007; Ilbert et al. 2010). If the galaxy merger rate is a function of stellar mass or luminosity (e.g. Lin et al. 2004; Bundy et al. 2005; de Ravel et al. 2009; Bridge et al. 2010), then one must be careful about comparing studies with different parent selection criteria. In an attempt to sample similar galaxies over a wide redshift range, the parent galaxy sample may be selected to be more massive than a fixed stellar mass (e.g. Bundy et al. 2009, Conselice et al. 2009, de Ravel et al. 2009, Jogee et al. 2009, Bridge et al. 2010) or by adopting an evolving luminosity selection based on a passive luminosity evolution (PLE) model in which galaxies of a fixed stellar mass are fainter at lower redshift due to passive aging of their stellar populations (e.g. Lotz et al. 2008, Lin et al. 2008, de Ravel et al. 2009, Shi et al. 2009).

We compare the number densities of galaxies selected with passive luminosity evolution assumptions (Fig. 2, upper panel) and with a fixed stellar mass (Fig. 2, lower panel). The number densities for the PLE cuts $M_B < -18.94 - 1.3z$ and $M_V < -19.8 - 1.0z$ and the fixed stellar mass cut $M_{star} \geq 10^{10} M_\odot$ are similar at $z < 1$, suggesting that the evolving luminosity selections of Lin et al. 2008, Lotz et al. 2008, Kartaltepe et al 2007, Shi et al. 2009, and the fixed stellar-mass selection of Bundy et al. 2009, Conselice et al. 2009, de Ravel et al. 2009, and López-Sanjuan et al. 2009 probe similar galaxy populations. However, the number density of galaxies selected by the de Ravel et al. (2009) $M_B < -18.77 - 1.1z$ cut is higher at higher z than the other selections. When a fixed luminosity ('no evolution') cut is adopted, as in Kartaltepe et al. 2007 and Rawat et al. 2008, the differences in the parent sample at $z \sim 1$ are even more significant, which could explain the difference in the derived evolution of the mergers. We will return to this issue in §5.4.

An additional complication is that merging galaxies increase in stellar mass and luminosity as they merge, as well as undergo shorter-lived starbursts. Therefore late-stage mergers and merger remnants will be more massive and luminous than their progenitors. Morphological disturbances are often late stage mergers whose nuclei are counted as a single objects, while close pairs are early-stage mergers (e.g. Lotz et al. 2008). Thus morphologically-disturbed mergers at a given mass/luminosity are drawn from a less-massive progenitor population than close pairs selected at the same mass/luminosity limit. In the worst case of equal-mass mergers, the morphologically-disturbed mergers will have progenitors 50% less massive and up to a magnitude fainter than close pairs. The inferred merger rate from morphologically-disturbed objects could be biased to higher values than the close-pair merger rate if the number density of merger progenitors increases with lower stellar mass. However, as we discuss in the next section, both $G - M_{20}$ and A are sensitive to minor mergers as well as major mergers. Therefore the difference between the typical (primary) progenitor's and the remnant's stellar mass is less than 25% for morphologically-selected samples, assuming a typical merger ratio 1:4. A related issue is short-lived luminosity brightening of both close pairs and morphologically-disturbed galaxies

from merger-induced starburst. This effect could bias luminosity-selected samples similarly, and give different merger rates than samples selected by stellar mass. However, merger simulations suggest that luminosity brightening in the rest-frame optical is mitigated by dust obscuration of the starbursts (Jonsson et al. 2006). In §5, we find little difference between the merger rates for luminosity and stellar-mass selected samples, implying that luminosity brightening does not introduce significantion biases to the merger rate.

Finally, it is also important to note that the standard selection of galaxy sample for galaxy merger studies (e.g. above a fixed stellar mass) is not well matched to the way that dark matter halos are selected from simulations for dark matter halo merger studies (e.g. above a fixed halo mass). We know that typical blue galaxies are not evolving purely passively, but form a significant number of new stars at $z < 1$ (e.g. Lilly et al. 1996 ; Noeske et al. 2007). Therefore the relationship between stellar mass and host dark matter halo mass also evolves with redshift (Zheng, Coil, & Zehavi 2007; Conroy & Wechsler 2009; Moster et al. 2010). Given that the co-moving number density of galaxies with stellar masses $> 10^{10} M_\odot$ or selected based on PLE assumptions is as much as a factor of four lower at $z \sim 1.5$ than $z \sim 0$, it is clear that neither of these galaxy samples select the progenitor and descendant galaxies across the range of redshifts.

Galaxy samples selected with a constant number density may do a better job of matching descendant-progenitor galaxies over a range of redshifts (van Dokkum et al. 2010; Papovich et al. 2010), and matching galaxies to constant mass halos (at $M_{halo} \sim 10^{11-12} M_\odot$; Zheng et al. 2007). This is not a perfect selection criterion, as it assumes galaxy mergers do not destroy significant numbers of galaxies and that stochasticity in the luminosity/mass evolution of galaxies does not strongly affect the sample selection. In §5.4, we present galaxy merger rates for parent galaxy samples selected with a roughly constant number density at $z < 1.5$, and compare these to the rates derived for the fixed stellar mass and PLE samples.

4. MERGER OBSERVABILITY TIMESCALES

Knowledge of the average merger observability timescale $\langle T_{obs} \rangle$ is crucial for calculating the galaxy merger rate. This timescale will depend upon the method used to select galaxy mergers, as close pairs pick out different merger stages from objects with disturbed morphologies. For a given merger system, the individual observability timescale will also depend on the parameters of the merger, such as the initial galaxy masses, morphologies and gas fractions, the merger mass ratio, the orbit, and the relative orientation of the merging galaxies. The initial properties of the merging system are difficult to reliably recover from observations of an individual merging system, particularly after the merger has progressed to late stages. Moreover, the observed merger population is a mixture of merger events with a broad distribution of parameters which may be evolving with redshift. Therefore the mean observability timescale $\langle T_{obs} \rangle$ given in Eqn. 3 should be treated as a cosmologically-averaged observability timescale weighted by the distribution of merger parameters at each epoch.

Because the observations of a given galaxy merger are essentially an instantaneous snapshot at a particular merger stage, we cannot know how long that merger event will exhibit disturbed morphology or other obvious merger indicators. And, depending on the merger stage and viewing angle, it can be difficult to determine its initial conditions. Therefore, the best way to determine how the morphology and projected separation of a merger progresses and how this depends on the merger conditions is by studying a large number of high-resolution numerical simulations of individual mergers where the initial merger conditions are systematically explored. Also, we do not yet have good observational constraints on the distribution and evolution of galaxy merger parameters such as gas fraction or mass ratio. Thus we will use theoretical predictions from three different global galaxy evolution models of the distribution of galaxy properties and their evolution to constrain the distribution of merger parameters with redshift.

In this section, we summarize the results of recent calculations of the individual observability timescales from a large suite of high-resolution disk-disk galaxy merger simulations for the $G - M_{20}$, A, and close pair methods. Then we examine the predicted distributions of two key merger parameters – baryonic gas fraction and mass ratio – and their evolution with redshift from three different cosmological-scale galaxy evolution models (Somerville et al. 2008; Croton et al. 2006; Stewart et al 2009b). Finally, we use these distributions to weight the individual observability timescales and derive the average observability timescales as a function of redshift $\langle T_{obs}(z) \rangle$ for each galaxy evolution model and approach to detecting galaxy mergers. We compare the predictions of the different galaxy evolution models and discuss the uncertainties associated with $\langle T_{obs}(z) \rangle$. The derived $\langle T_{obs}(z) \rangle$ are applied to the observed merger fractions described in §3 to compute merger rates in §5.

4.1. Merger Timescales from Dusty Interacting Galaxy GADGET/SUNRISE Simulations

The individual merger observability timescales T_{obs} were calculated for a large suite of high-resolution N-body/hydrodynamical galaxy merger simulations in Lotz et al. 2008b, 2010a, b (also known as DIGGSS, Dusty Interacting Galaxy GADGET/SUNRISE Simulations; see http://archive.stsci.edu/prepds/diggss for simulation images and morphology measurements). Each GADGET simulation tracks the merger of two disk galaxies within a box of $\sim (200 \text{ kpc})^3$ with a spatial resolution ~ 100 pc and a particle mass $\sim 10^5 M_\odot$, over a several billion year period in ~ 50 Myr timesteps. Cold gas is converted into stars assuming the Kennicutt-Schmidt relation (Kennicutt 1998). The effects of feedback from supernovae and stellar winds using a sub-resolution effective equation of state model is included, but feedback from active galactic nuclei (e.g. Di Matteo et al. 2008) is not. The full suite of simulations span a range of initial galaxy masses and mass ratios, gas fractions, and orientations and orbital parameters and are described in detail in Cox et al. 2006, 2008. The DIGGSS simulations do not include any $f_{gas} < 0.2$ simulations or spheroidal merger simulations.

The GADGET predictions for the ages, metallicities, and 3-D distribution of stars and gas for each simula-tion and time-step were run through the Monte-Carlo radiative transfer code SUNRISE to simulate realistic ultraviolet-optical-infrared images, including the effects of star-formation, dust, and viewing angle. The details of the SUNRISE code and the predicted effects of dust on the integrated spectral energy distributions are described in Jonsson 2006, Jonsson, Groves, & Cox 2010. In Lotz et al. (2008b, 2010a, 2010b), the simulated broad-band SDSS g images were used to calculate the time during which each individual galaxy merger simulation would be counted as a merger candidate by the quantitative morphology $G - M_{20}$ and asymmetry methods. We also calculate close pair timescales for several different projected separation criteria ($5 < R_{proj} < 20$, $10 < R_{proj} < 30$, $10 < R_{proj} < 50$, and $10 < R_{proj} < 100$ kpc h^{-1}); all simulations have merging galaxies with relative velocities less than 500 km s^{-1}. Note that for the close pair and $G - M_{20}$ methods, the observability windows are not contiguous in time and therefore the observability time is the sum of the times when the merger is selected, e.g. as a close pair before and after the first pass.

We found that, for a given method, T_{obs} depended most on the mass ratio of the merger (Lotz et al. 2010a) and on the gas fractions of initial galaxies (Lotz et al. 2010b). Orbital parameters (eccentricity, impact parameters) and total mass of the initial galaxies had little effect on T_{obs} for morphological disturbances. We will refer to the baryonic mass ratio of the merger $M_{satellite}/M_{primary}$, where major mergers have baryonic mass ratios between 1:1 and 1:4 and minor mergers have baryonic mass ratios less than 1:4. We have chosen to characterize the merger mass ratio by the initial baryonic mass ratio rather than total or stellar mass ratio as a compromise between observational and theoretical limitations. The total mass ratio of mergers is difficult to estimate (or even define) observationally because this requires a dynamical estimate of mass associated with each interacting galaxy. On the other hand, the stellar masses and stellar mass ratios predicted by cosmological galaxy evolution models can be quite sensitive to the uncertain physics of star formation and feedback (see, for example, Benson et al. 2003). As a result, a galaxy merger with a total mass ratio of 1:3 may correspond to a stellar mass ratio of anywhere from 1:10 to 1:2 (Stewart 2009a). While baryonic mass ratios suffer the same complication, one may expect the ratio of baryonic-to-total mass to vary less strongly with redshift, since higher gas fractions at earlier times help offset the proportionately smaller stellar-to-total masses of $\sim L^*$ galaxies.

Likewise, we characterize the merger gas fraction as the initial fraction of the baryons in cold gas. We define the initial baryonic gas fraction f_{gas} of the merger as

$$f_{gas} = \frac{(M_{gas,1} + M_{gas,2})}{(M_{gas,1} + M_{gas,2} + M_{star,1} + M_{star,2})} \quad (7)$$

This is the average gas fraction of the system prior to the merger, when the galaxies first encounter each other. Because these simulations do not accrete additional gas and gas is converted into stars, the baryonic gas fraction at the final merger is lower than the initial value. For this work, we use a sub-set of DIGGSS which have parabolic orbits, tilted prograde-prograde orientations and initial galaxy parameters tuned to match
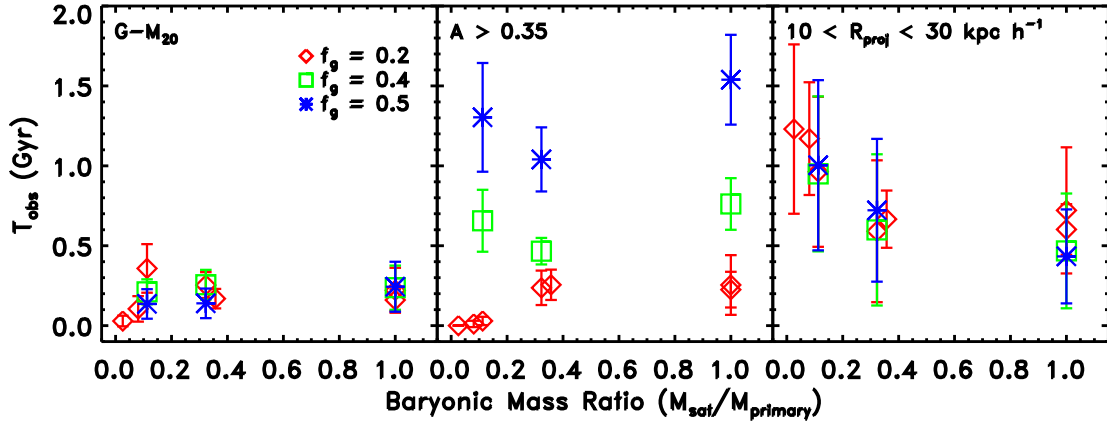
FIG. 3.— The observability timescales T_{obs} for individual prograde-prograde disk-disk galaxy merger simulations v. baryonic mass ratio ($M_{primary}/M_{satellite}$) from Lotz et al. 2010a,b. The simulations were run with three different baryonic gas fractions $f_{gas} = 0.2$ (red diamonds: G3G3Pt, G3G2Pt, G3G1Pt, G3G0Pt, G2G2Pt, G2G1Pt, G2G0Pt), 0.4 (green squares: G3gf1G3gf1, G3gf1G2, G3gf1G1) , and 0.5 (blue asterisks: G3gf2G3gf2, G3gf2G2, G3gf2G1).
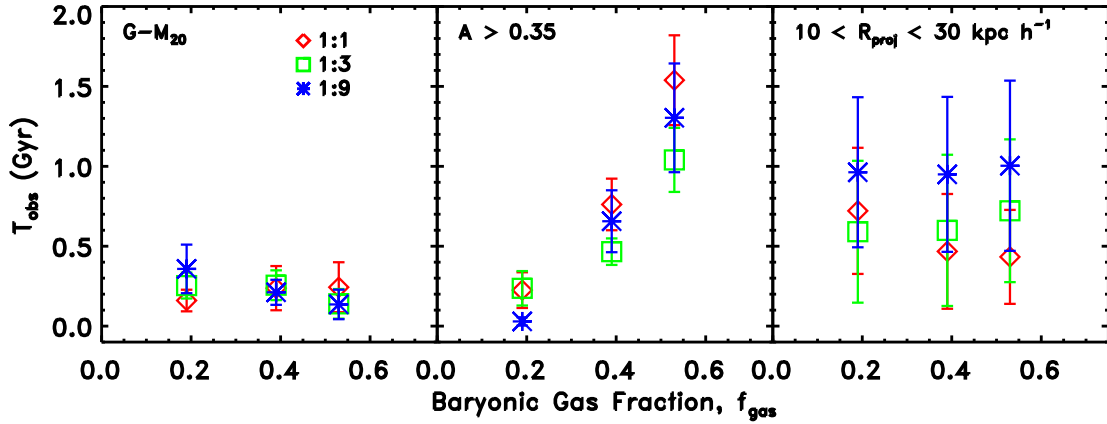

FIG. 4.— The observability timescales T_{obs} for individual prograde-prograde disk-disk galaxy merger simulations v. baryonic gas fraction f_{gas} from Lotz et al. 2010a,b. Here, the points designate three different baryonic mass ratios $M_{satellite}/M_{primary}$ 1:1(red diamonds: G3G3Pt, G3gf1G3gf1, G3gf2G3gf2), 3:1 (green squares: G3G2Pt, G3gf1G2, G3gf2G2), and 9:1 (blue asterisks: G3G1, G3gf1G1, G3gf2G1).

SDSS galaxies, but span a range of galaxy mass ($M_{star} \sim 1 \times 10^9 - 5 \times 10^{10} M_\odot$) and baryonic mass ratios (1:1 - 1:39): G3G3Pt, G3G2Pt, G3G1Pt, G3G0Pt, G2G2Pt, G2G1Pt, G2G0Pt. These simulations have gas fractions tuned to local galaxies, with the initial baryonic gas fractions $f_{gas} \sim 0.2$. We also use the subset of DIGGSS which have the same parabolic orbits, tilted prograde-prograde orientations, and mass ratios but higher gas fractions ($f_{gas} \sim 0.4$, 0.5) : G3gf1G3gf1, G3gf1G2, G3gf1G1, G3gf2G3gf2, G3gf2G2, G3gf2G1. See Lotz et al. (2010a, b) and Cox et al. (2008) for more details of these simulations.

In Figures 3 and 4, we show how the individual observ-

ability timescales T_{obs} for $G - M_{20}$, A, and close pairs with $10 < R_{proj} < 30$ kpc h^{-1} depend on baryonic mass ratio and f_{gas}. Note that these are averaged over 11 different viewing angles (see Lotz et al. 2008b). The error-bars on T_{obs} in Figures 3 and 4 are the standard deviation with viewing angle of T_{obs} for each simulation. $G-M_{20}$ and close pair observability timescales are largely independent of gas fraction but are sensitive to mass ratio, while asymmetry A is sensitive to both gas fraction and mass ratio. $G - M_{20}$ detects mergers with baryonic mass ratios between 1:1 and at least 1:10, and does not show a strong correlation of T_{obs} with baryonic mass ratio above 1:10. Mergers are not found with the $G - M_{20}$

criteria for the two simulations with baryonic mass ratios less than 1:10 (G2G0Pt, G3G0Pt), therefore we conclude that $T_{obs} \sim 0$ for mergers at these mass ratios. The simulations imply that $G - M_{20}$ detects mergers at the stage when two bright nuclei are enclosed in a common envelope, and that satellites with masses greater than a tenth of the primary galaxies are bright enough to be detected (see Lotz et al. 2008a, Lotz et al 2010a for discussion).

Dynamical friction and the effects of projection largely drive the close pair timescales, hence their insensitivity to f_{gas}. The close pair timescales are correlated with mass and mass ratio such that minor mergers appear as close pairs for a longer period of time than major mergers, as do lower-mass major mergers (Table 5 in Lotz et al. 2010a).

The behavior of A observability timescales is more complicated because of their dependence on both mass ratio and gas fraction. The simulations suggest that high asymmetries are the result of large-scale disturbances, including bright star-forming tidal tails and dust lanes, thus asymmetry is higher for more gas-rich mergers which are more likely to form strong tidal features (see Lotz et al. 2010b). At gas fractions expected for typical local disk galaxies ($f_{gas} \sim 0.2$), A detects primarily major mergers with baryonic mass ratios between 1:1 and 1:4, and has $T_{obs} \sim 0$ for more minor mergers with baryonic mass ratios 1:10 (Figure 3, red points, center panel). But for simulations with $f_{gas} \geq 0.4$, A detects both 1:1-1:4 major mergers and 1:10 minor mergers (Figure 3, center panel, green and blue points). The observability timescale for A is strongly correlated with f_{gas} (Figure 4, center panel), with high gas fraction mergers showing high asymmetries for significantly longer periods of time than low gas fraction mergers. Therefore knowledge of both the merger gas fraction and mass ratio distributions is required to estimate $\langle T_{obs} \rangle$ for asymmetry.

For this work, we will ignore the effect of the orbital parameters and relative orientations of the merging galaxies on the observability timescales. All of the simulation timescales adopted here are for the G-series prograde-prograde orientations, with $e = 0.95$ and pericentric distances $\sim 0.01 - 0.05$ times the viral radii of the progenitors. In Lotz et al. (2008b) and (2010a), we found that different orbits and orientations had a weak effect on the observability timescales for $G - M_{20}$ and A. However, galaxies merging on circular orbits or with large impact parameters were identified as close pairs for 15-40% longer than parabolic orbits with smaller impact parameters, depending on the projected separation requirements. Large-scale numerical simulations find that the majority of dark-matter halo mergers are parabolic as opposed to circular (Khochfar & Burkert 2006; Benson 2005; Wetzel 2010), with only modest evolution in the typical orbital eccentricity out to $z \sim 1.5$ (Wetzel 2010). Our adopted e is consistent with the mean value for dark matter halo -satellite mergers from Wetzel (2010; $e \sim 0.85$), while our pericentric distances are smaller than mean ($\sim 0.13\ R_{vir}$). If true pericentric distances are significantly larger than our assumptions here, our simulations imply that this could systematically increase the merger timescales (and decrease merger rates) by up to 10-40% for close pairs and a factor of 3-4 for $G - M_{20}$ selected major mergers (Lotz et al. 2008b).

4.2. *Predicted Distribution of Merger Properties*

We calculate the cosmologically-averaged observability timescale $\langle T_{obs}(z) \rangle$ for each method for finding mergers from the individual T_{obs} given in Figures 3 and 4 and assumptions about the distribution of galaxy merger mass ratios and f_{gas} as follows:

$$\langle T_{obs}(z) \rangle = \sum_{i,j} w_{i,j}(z) \times T_{i,j} \qquad (8)$$

where $w_{i,j}(z)$ is the fraction of mergers at redshift z with baryonic mass ratio i and baryonic gas fraction j, and $T_{i,j}$ is the observability timescale for a merger with baryonic mass ratio i and baryonic gas fraction j. (Although the timescales do not change much with progenitor mass, in practice we also sum over two bins in primary progenitor baryonic mass based on the input simulation primary galaxy masses of 2.0×10^{10}, $6.2 \times 10^{10} M_{\odot}$).

We currently have very little empirical knowledge of the distribution of baryonic mass ratios or gas fractions for merging galaxies. Therefore we assume the relative distributions of mass ratios, gas fractions, and mass as a function of redshift predicted by three different cosmological-scale galaxy evolution models: Somerville et al. 2008 [S08]; Croton et al. 2006 [C06]; and Stewart et al. 2009b [St09]. Note that for the timescale calculations, we make use of only the *relative* distributions of merger properties from these simulations and therefore are independent of their predicted galaxy merger rates.

Each of these models starts with a mass distribution and merger history (merger tree) for the dark matter central and sub-halos. S08 uses an analytically-derived dark matter merger tree (Somerville & Kolatt 1999) with a Sheth & Tormen (1999) dark matter halo mass function; the C06 and St09 merger trees are derived from N-body simulations (the Millennium Simulation from Springel et al. 2005 and an Adaptive Refinement Tree N-body simulation from A. Klypin described in Stewart et al. 2008, respectively). These dark matter halos are populated with galaxies, either via a semi-analytic approach that adopts physical prescriptions for galaxy formation (C06, S08) or via a semi-empirical approach that matches the expected clustering and abundances of dark matter halos to the observed galaxy population (St09). In the semi-analytical models, gas cools onto the dark matter halos and is converted into stars assuming the Kennicutt-Schmidt law (Kennicutt et al. 1998). The semi-analytic models also adopt similar prescriptions for feedback from supernovae and both high-luminosity quasars and lower luminosity active galactic nuclei. The S08 models are tuned to match the gas fractions of local galaxies. By contrast, the semi-empirical model of St09 assigns the stellar masses and gas masses of galaxies based on observationally-derived correlations, with stellar masses following the abundance matching technique of Conroy & Wechsler (2009), and cold gas fractions following an empirical fit to the results of McGaugh (2005) at $z \sim 0$ and Erb et al. (2006) at $z \sim 2$ (see Stewart et al. 2009a,b for additional details).

For each galaxy evolution model, we select galaxy mergers with total stellar masses $(M_{star,1} + M_{star,2}) \geq 10^{10} M_{\odot}$, baryonic mass ratios $\geq 1:10$, and $0 < z < 1.5$. The galaxy stellar mass functions at $z < 1.5$ from all of
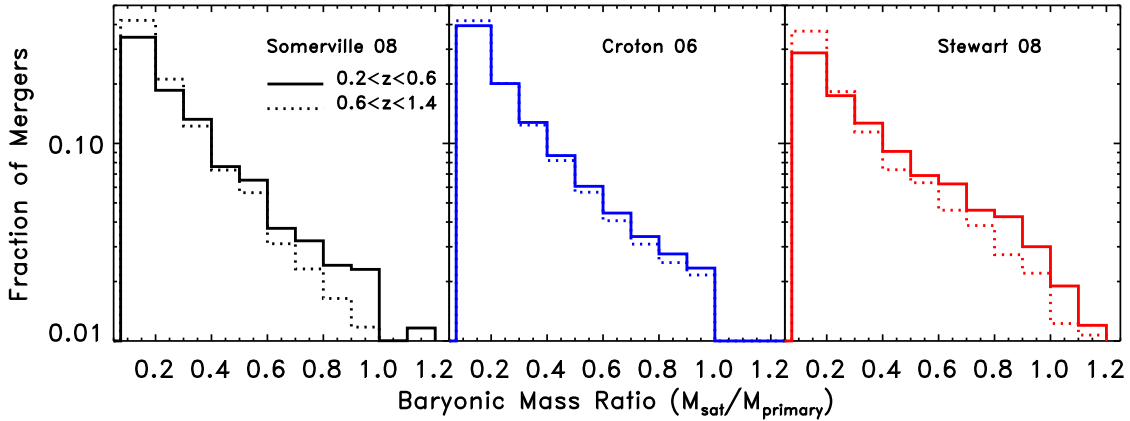
Fig. 5.— The normalized distribution of baryonic mass ratios for galaxy mergers selected from the Somerville et al. 2008 (black histogram), Croton et al. 2006 (blue), and Stewart et al. 2009b (red) models. The mergers were selected to be in two redshift bins ($0.2 < z < 0.6$; solid lines; $0.6 < z < 1.4$ dashed lines), with total stellar masses ($M_{star,1} + M_{star,2}$) $> 10^{10}M_\odot$), and baryonic mass ratios $\geq$ 1:10. There is good agreement between all three models, and little evolution in the distribution with redshift. (Baryonic mass ratios greater than unity arise when the more massive galaxy has less baryons but more dark matter than its companion).
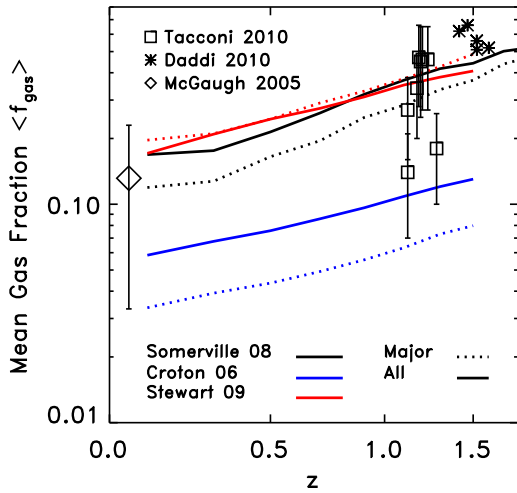
$z < 1.5$ and for galaxies with masses above $\sim 10^{10}M_\odot$ (see Fontanot et al. 2009, Kitzbichler & White 2007).

We compare the distribution of baryonic mass ratios and gas fractions for the three models in Figures 5 and 6. In Figure 5, we find that the S08, St09, and C06 models predict similar baryonic mass ratio distributions despite the different derivations of the dark matter halo mass function, merger tree, and baryonic masses. We find a small increase in the relative fraction of minor mergers ($M_{sat}/M_{primary} < 0.25$) at higher redshifts for the S08 and St09 models, while C06 predicts no change in the mass ratio distribution.

However, the models make different predictions about the merger gas properties (Figure 6). In all the models, f_{gas} increases significantly with redshift such that the mean baryonic gas fraction of the mergers roughly doubles from $z = 0$ to $z = 1$. The mean f_{gas} values for all 1:1 - 1:10 mergers predicted by the S08 and St09 models are in good agreement. On the other hand, the mean f_{gas} in the C06 models is much lower at all redshifts. Both S08 and C06 predict that major mergers with baryonic mass ratios less than 1:4 have lower mean gas fractions than minor mergers. On the other hand, St09 predict that major mergers have f_{gas} similar to the overall merger population.

In Figure 6, we also compare the predicted mean gas fractions to recent measurements of the cold gas fraction for massive disk galaxies at $z \sim 1 - 1.5$ from Tacconi et al. (2010) and Daddi et al. (2010). Although these pioneering studies have small and biased samples, they indicate that the typical baryonic gas fractions of massive disk galaxies are several times higher at $z \sim 1 - 1.5$ than locally (e.g McGaugh et al. 2005), in reasonable agreement with the Somerville et al. (2008) and Stewart et al. (2009b) models.

For each model, we compute the weight $w_{i,j}(z)$ for three bins in baryonic mass ratio and four bins in f_{gas} for $\delta z = 0.2$ redshift bins from $z = 0$ to $z = 1.6$, normalized to all merging systems in each redshift bin with ($M_{star,1} + M_{star,2}$) $\geq 10^{10}M_\odot$ and baryonic mass ratios

Fig. 6.— The predicted mean baryonic gas fraction $\langle f_{gas} \rangle$ v. redshift for 1:1 - 1:10 baryonic mass ratio mergers (solid) and major 1:1-1:4 baryonic mass ratio mergers (dashed line). All models predict strong evolution in $\langle f_{gas} \rangle$ with redshift, but the Somerville et al. 2008 (black lines) and Stewart et al. 2009b (red lines) mergers have higher $\langle f_{gas} \rangle$ than the Croton et al. 2006 models (blue lines). For comparison, we have plotted the observed f_{gas} at $z > 1$ for the Tacconi et al. 2010 (squares) and Daddi et al 2010 (asterisks) samples, and the average f_{gas} and standard deviation for the McGaugh 2005 sample of local $M_{star} > 10^{10}M_\odot$ disk galaxies (diamond).

the models are in good agreement with each other. St09 adopts the sub-halo mass - stellar mass matching relationship from Conroy & Wechsler (2009), based upon the observed stellar mass functions at $0 < z < 2$ (Bell et al. 2003, Panter et al. 2007, Dory et al. 2005, Borsch et al. 2006, Pérez-González et al. 2008, Fontana et al. 2006). The S08 and C06 predictions for the galaxy stellar mass functions (assuming a Chabrier initial mass function and Bruzual & Charlot 2003 SEDs) are found to be in good agreement with these same observed measurements at
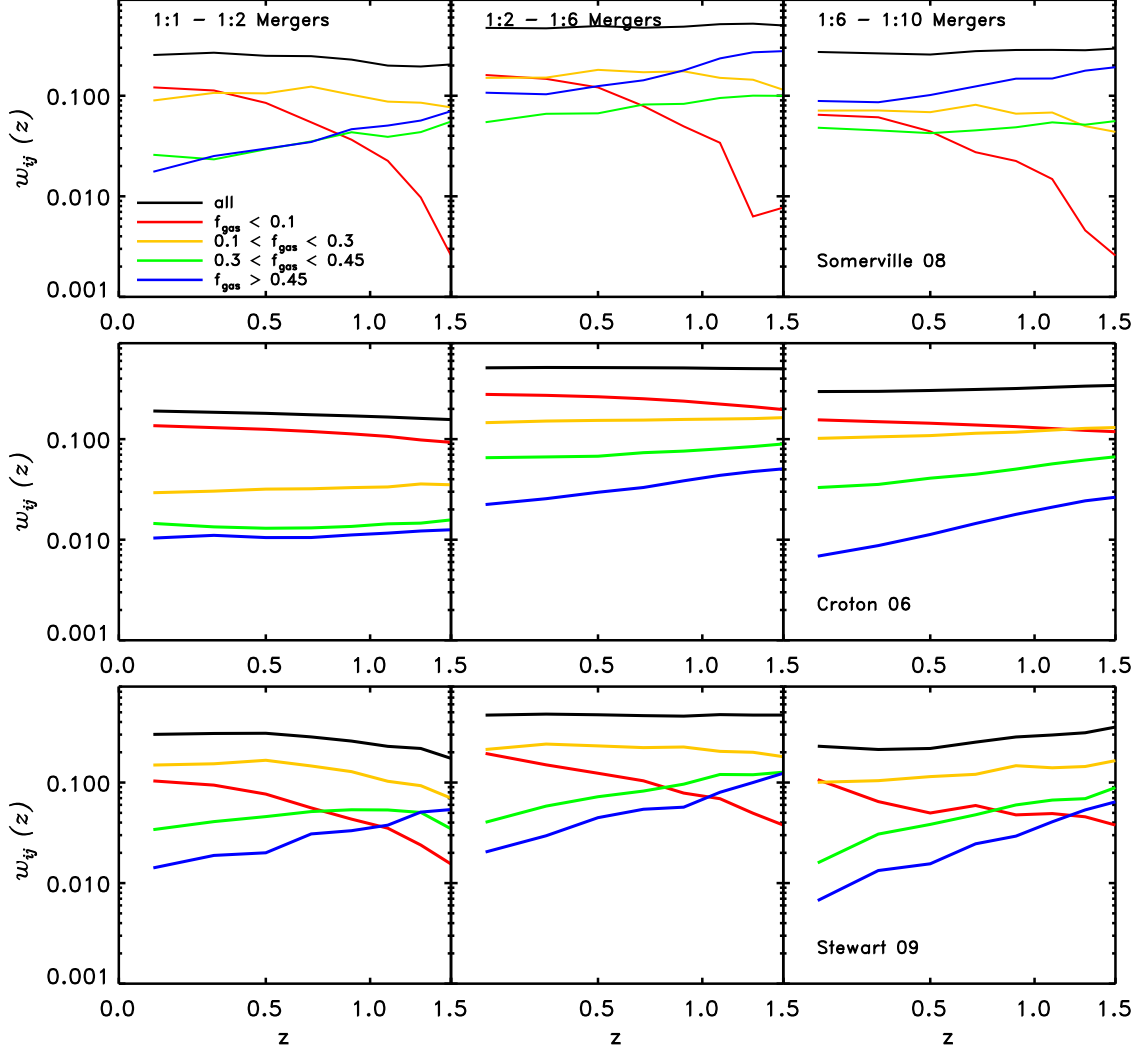
FIG. 7.— The fraction of mergers $w_{i,j}$ with baryonic mass ratio i and baryonic gas fraction j v. redshift from the Somerville et al. (2008) models (top panels), the Croton et al. (2006) models (middle panels), and Stewart et al. (2009b) models (bottom panels). The weights have been calculated for three baryonic mass ratio bins (1:1-1:2, left panels; 1:2-1:6, center panels; 1:6-1:10, right panels) and four baryonic gas fraction bins ($f_{gas} < 0.1$, red lines; $0.1 < f_{gas} < 0.3$, orange lines; $0.3 < f_{gas} < 0.45$, green lines; $f_{gas} > 0.45$, blue lines.) The black lines in each panel show the fraction of mergers of all gas fractions for that panel's mass ratio bin.

$\geq 1:10$ (Figure 7). The spacing of these bins is determined by the simulation parameter space for the SDSS-motivated galaxy mergers: 1:1 - 1:2 (major), 1:2-1:6 (intermediate), and 1:6-1:10 (minor) baryonic mass ratio bins; and 0.0-0.1, 0.1-0.3, 0.3-0.45, and 0.45-1.0 f_{gas} bins. The three baryonic mass ratio bins are plotted in separate panels (major:left, intermediate:center, and minor: right). The four f_{gas} bins are plotted with different color lines in each mass ratio panel. The resulting weights are shown for the three galaxy evolution models (S08: top, C06: middle, St09: bottom).

For all three models, the baryonic mass ratio distribution changes little with redshift, and intermediate mass ratio mergers (1:2 - 1:6; middle panels) are 50% of the total (1:1 -1:10) merger population at all redshifts. The predicted weights $w_{i,j}(z)$ vary most in the predicted distribution and evolution of merger gas fractions. All three

models predict that lower gas fraction mergers dominate the $z = 0$ merger population (red and yellow lines). However, S08 predicts strong evolution in the gas properties of mergers, such that by $z \geq 1$, the merger population is dominated by high gas fraction ($f_{gas} > 0.45$) intermediate and minor mergers (blue lines, middle and right panels). Because C06 predicts low mean f_{gas} at $z < 1.5$, they predict that the lowest gas fraction mergers continue to dominate at $z > 1$ (red lines). Like S08, the St09 model predicts higher mean f_{gas} at $z \geq 1$. But St09 has a different distribution of f_{gas} at a given redshift. St09 has fewer very gas-rich mergers and more very gas-poor mergers at $z \sim 1$, and predicts that most mergers at $0 < z < 1.5$ have intermediate $f_{gas}(\sim 0.2)$ in all mass ratio bins (yellow lines). As we will discuss in the next section, the relative frequency of gas-rich intermediate and minor mergers at $z \geq 1$ has important

implications for the interpretation of asymmetric galaxies at this epoch.

4.3. Average Merger Timescales $\langle T_{obs}(z) \rangle$

We compute $\langle T_{obs}(z) \rangle$ for $G - M_{20}$, asymmetry, and close pairs with $5 < R_{proj} < 20$, and $10 < R_{proj} < 30$ kpc h^{-1}, using Eqn. 8, the $T_{i,j}$ computed from the GADGET-SUNRISE simulations as a function of baryonic mass ratio and gas fraction (Figures 1 and 2), and the relative weights $w_{i,j}$ computed from each of the cosmological galaxy evolution models. These cosmologically-weighted timescales $\langle T_{obs}(z) \rangle$ are plotted as a function of redshift for the three different models for each method for finding mergers (Figures 8 and 9).

The relative weights $w_{i,j}$ are adjusted for the mass ratio sensitivity for each technique, so that the resulting merger rates are not extrapolated to mass ratios below what is detected. Therefore the weights for $G - M_{20}$ and A are normalized for all mergers with baryonic mass ratios between 1:1 and 1:10, and assume no mergers with mass ratios $\leq$ 1:10 are detected by these methods (same as Fig. 7). The weights for close pairs are normalized to baryonic mass ratios between 1:1 and 1:4 or between 1:1 and 1:2, depending on the stellar mass and luminosity ratios adopted by the studies presented here (Table 1).

Both the gas fraction and morphological make-up of merger progenitors are expected to change significantly between $0 < z < 1.5$. The number density of red sequence (presumably gas-poor) galaxies more massive than $\sim 10^{10} M_\odot$ roughly doubles over this time period (Bell et al. 2004, Faber et al. 2007), and the fraction of bright galaxies which are spheroid dominated increases from $\sim 20\%$ at $z \sim 1.1$ to $\sim 40\%$ at $z \sim 0.3$ (Lotz et al. 2008a). The cold gas fractions measured for small numbers of disk galaxies at $z \sim 1 - 1.5$ are $\sim 40\%$, three times higher than today's $\sim 10\%$ (Tacconi et al. 2010; Daddi et al. 2010; McGaugh 2005).

For $G - M_{20}$ and close pairs, the individual observability timescales $T_{i,j}$ are not a strong function of f_{gas}. We assume that $f_{gas} < 0.1$ mergers have the same observability timescales as $f_{gas} = 0.2$ mergers of the same mass ratio. We note that gas-free spheroid-spheroid merger simulations presented in Bell et al. (2005) imply $\sim$0.2 Gyr timescales for visual classification of double nuclei, consistent with our adopted $G - M_{20}$ timescale for $f_{gas} < 0.1$.

However, the A timescales are a strong function of f_{gas}. Therefore, we compute upper and lower limits to $\langle T_{obs}(z) \rangle$ by assuming that that $f_{gas} < 0.1$ mergers have the same observability timescales as $f_{gas} = 0.2$ mergers (Figure 9; upper limit, solid lines) and by assuming that $f_{gas} < 0.1$ mergers are not detected by A (Figure 9: lower limit, dotted lines). We note that Bell et al. (2006) found visual-classification timescales for gas-poor spheroid-spheroid major merger simulations of $T_{obs} \sim 0.15$ Gyr, intermediate between the $T_{obs} = 0$ and $T_{obs} \sim 0.3$ Gyr for $f_{gas} = 0$ adopted here.

The cosmologically-averaged timescales for close pairs do not evolve with redshift and do not depend on the adopted cosmological galaxy evolution model (Fig. 8). This is not surprising given that the close pair timescales do not depend on gas fraction (which evolves strongly with redshift). The individual close pair timescales do depend on mass ratio, but the relative distribution of

mass ratios is not predicted to evolve with redshift. The timescales for close pairs selected with baryonic mass ratios between 1:1 and 1:4 are ~ 0.33 Gyr for $5 < R_{proj} < 20$ kpc h^{-1}, and ~ 0.63 Gyr for $10 < R_{proj} < 30$ kpc h^{-1} (Table 1; Figure 8).

We find that $\langle T_{obs}(z) \rangle$ for $G - M_{20}$ is also very similar for all three model weights, and does not evolve with redshift. This is not surprising as $G - M_{20}$ T_{obs} does not correlate with f_{gas} nor baryonic mass ratio between 1:1 and 1:10. Therefore, the $G - M_{20}$ observability timescales are not sensitive to the underlying assumptions about the distribution of merger gas fractions or mass ratios. For mergers with stellar masses $\geq 10^{10} M_\odot$ at $0 < z < 1.5$, $\langle T_{obs}(z) \rangle$ is ~ 0.21 Gyr for $G - M_{20}$ (Table 2; Figure 9 upper panel).

The cosmologically-averaged timescales for asymmetry are the most sensitive to the assumptions about the joint distribution of merger gas fractions and mass ratios (Figure 9). The uncertainty in the asymmetry timescales of $f_{gas} < 0.1$ gas-poor mergers changes $\langle T_{obs}(A) \rangle$ by less than 0.1 Gyr (dotted lines), and therefore is not a major contributor to the uncertainty in $\langle T_{obs}(A, z) \rangle$. However, the $\langle T_{obs}(A, z) \rangle$ calculated with the S08 weights (black lines) are significantly higher than those calculated with the C06 (blue lines) and St09 (red lines) weights. This arises from the strong dependence of A timescales on the f_{gas} and the different predictions for the distribution of $f_{gas}(z)$ for the different models. The strong evolution of the mean f_{gas} and higher frequency of very gas-rich minor mergers predicted by S08 result in the strong evolution of $\langle T_{obs}(A, z) \rangle$ with redshift. The low mean f_{gas} and its weak evolution predicted by C06 results in short $\langle T_{obs}(A, z) \rangle$ that evolves weakly with redshift. The St09 models predict similar evolution in the mean f_{gas} to S08, but has fewer high gas fraction intermediate/minor mergers, and therefore predicts lower values for $\langle T_{obs}(A, z) \rangle$.

In summary, the average observability timescales for $G - M_{20}$ and close pairs are not expected to evolve with redshift between $0 < z < 1.5$, and are relatively insensitive to the distribution of merger properties. The average observability timescales for A, on the other hand, are expected to increase between $0 < z < 1.5$ as the mean gas fraction of mergers increase, and are highly sensitive to both the distribution of merger gas fractions and mass ratios. If the typical gas fractions of galaxy mergers at $z \geq 1$ are as high as 0.4, as suggested by recent molecular gas observations, then typical timescales for identifying a merger as asymmetric should more than double. If very gas-rich minor mergers are also more likely at $z \geq 1$, than the contribution of minor mergers to the asymmetric galaxy population will also increase with redshift.

5. GALAXY MERGER RATES

In the previous section, we calculated cosmologically-averaged merger observability timescales that account for differences in merger identification techniques and the distribution of merger mass ratio and gas fraction. In this section, we use these improved estimates of $\langle T_{obs}(z) \rangle$ to re-analyze recent studies of the evolution of the galaxy mergers (reviewed in §3). In Tables 1, 2, and 3, we give $\langle T_{obs}(z) \rangle$ calculated specifically for each merger study/technique, the resulting fractional merger rates, $\Re_{merg}(z)$, and the merger rates per co-moving vol-
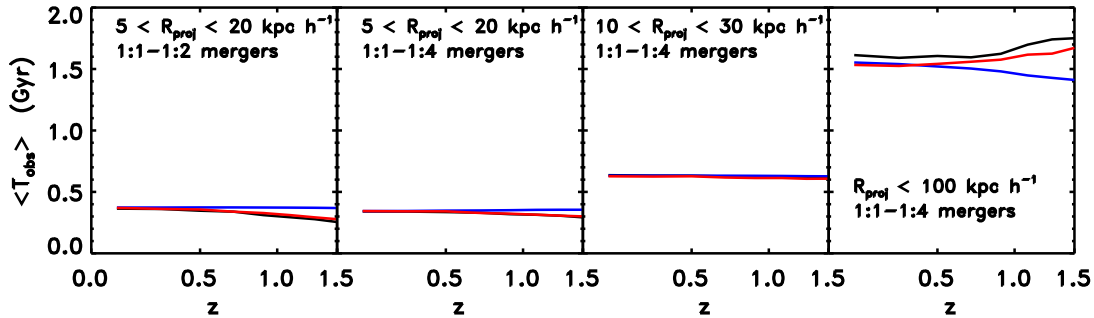
FIG. 8.— The average observability timescale $\langle T_{obs} \rangle$ for several close pair selection criteria: $5 < R_{proj} < 20$ kpc h^{-1} and 1:1 - 1:2 baryonic mass ratio; $5 < R_{proj} < 20$ kpc h^{-1} and 1:1 - 1:4 baryonic mass ratio; $10 < R_{proj} < 30$ kpc h^{-1} and 1:1 - 1:4 baryonic mass ratio; $R_{proj} < 100$ kpc h^{-1} and 1:1 - 1:4 baryonic mass ratio. The close pair timescales are very similar for all these models.
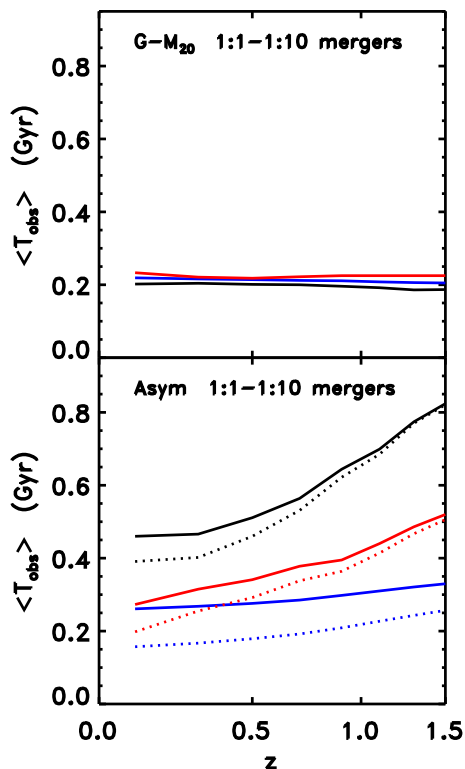

FIG. 9.— The average observability timescale $\langle T_{obs} \rangle$ for $G-M_{20}$-selected mergers (top) and asymmetric mergers (bottom) with baryonic mass ratios between 1:1 and 1:10. $G - M_{20}$ timescales are independent of the assumptions about the distribution of f_{gas}. Asymmetry timescales evolve most strongly for the S08 model f_{gas} distribution (black lines), which assumes many gas-rich minor mergers at $z \geq 1$. Asymmetry timescales evolve weakly for the C06 model f_{gas} distribution (blue lines), which assumes low f_{gas} mergers at $0 < z < 1.5$. The A timescales predicted by the St09 models also evolve strongly with redshift, but are shorter than S08 because St09 has fewer very gas-rich mergers. The dotted lines assume that $f_{gas} < 0.1$ mergers are not detected by A (see text).

ume, $\Gamma_{merg}(z)$. For close pairs and $G - M_{20}$, we adopt the S08 timescales, given that there is little variation in timescales with cosmological merger distributions. For asymmetry, different gas fraction assumptions result in very different $\langle T_{obs}(z) \rangle$. There are also very different

literature values for the asymmetry fractions, hence we treat each set of observations/model timescales separately.

We calculate both $\Gamma_{merg}(z)$ and $\Re_{merg}(z)$ for close pairs, $G-M_{20}$, and A selected mergers. We focus primarily on the galaxy merger rates for samples selected with an evolving luminosity cut (PLE) or fixed stellar mass cut (M_{star}) in §5.1-5.3. In §5.4 we discuss the implications of selecting parent galaxy samples with a constant number density. In §5.5 we compare our results for stellar-mass selected merger rates to the predictions of several galaxy evolution models. In general, we fit the galaxy merger rates with power-laws of the form $C \times (1 + z)^{\alpha}$.

5.1. The Major Merger Rate: Close Pairs

The close pair studies included in this paper select galaxies with luminosity or stellar mass ratios less than 1:2 or 1:4. Although luminosity brightening of an interacting satellite galaxy may cause the measured luminosity ratio to be less than the stellar or baryonic mass ratio (e.g. Bundy et al. 2004), we assume that this sample primarily probes major mergers with baryonic mass ratios roughly comparable to their luminosity or stellar mass ratios.

When samples with similar parent selection criteria are compared, we find that the merger rates derived from various close pair studies are remarkably consistent (Figure 10). However, the evolution of the merger rate depends on whether one calculates the merger rate per galaxy ($\Re$) or the merger rate per unit volume (Γ). The best-fit evolution in $\Gamma_{pairs}(z)$ is weaker than $\Re_{pairs}(z)$ because the evolution in $n_{gal}(z)$ is opposite to the trend in $\Re_{pairs}(z)$ (see Figures 1 and 2). The major merger rate (Γ_{pairs} or $\Re_{pairs}$) and its evolution with redshift are similar for the stellar-mass and evolving luminosity selected samples, suggesting that luminosity-brightening does not significantly bias the luminosity-selected merger samples. In the left hand side of Figure 10, we plot Γ and $\Re$ for 1:1 - 1:4 pairs with $M_{star} > 10^{10} M_{\odot}$ from the Bundy et al. (2009) study (blue circles) and de Ravel et al. (2009) study (black circles). Despite being drawn from different fields with different close pair criteria, these agree well once the corresponding observability timescales are applied. The best fit volume-averaged merger rate $\Gamma_{pairs,M_{star}}(z)$ (blue line, top left panel) and fractional merger rate $\Re_{pairs,M_{star}}(z)$ (blue line, bottom

TABLE 1
Close Pair Fractions and Merger Rates

z	N_c	f_{pair}	n_{gal} $[10^{-3}\ \mathrm{Mpc}^{-3}]$	$\langle T_{obs}\rangle_{S08}$ [Gyr]	$\langle T_{obs}\rangle_{C06}$ [Gyr]	$\langle T_{obs}\rangle_{St09}$ [Gyr]	$\Re_{merg,S08}$[a] $[\mathrm{Gyr}^{-1}]$	$\Gamma_{merg,S08}$[a] $[10^{-3}\ \mathrm{Gyr}^{-1}\ \mathrm{Mpc}^{-3}]$
				Luminosity-selected Pairs				
Patton & Atfield 2008; $5 < R_{proj} < 20$ kpc h^{-1}; $1 < L_{primary}/L_{sat} < 2$; $\Delta V < 500$ km s^{-1}; $-22 < M_r < -18$								
0.05	0.021 ± 0.001	$\cdots$	9.55 ± 0.07	0.36	0.37	0.37	0.0175 ± 0.0008	0.17 ± 0.01
Lin et al. 2008; $10 < R_{proj} < 30$ kpc h^{-1}; $1 < L_{primary}/L_{satellite} < 4$; $\Delta V < 500$ km s^{-1}; $-21 < M_B + 1.3z < -19$								
0.12	0.054 ± 0.005	0.072 ± 0.007	6.14 ± 0.52	0.64	0.63	0.63	0.068 ± 0.007	0.41 ± 0.05
0.34	0.041 ± 0.011	0.063 ± 0.017	4.72 ± 2.30	0.63	0.63	0.63	0.060 ± 0.016	0.28 ± 0.16
0.58	0.063 ± 0.014	0.083 ± 0.018	5.00 ± 0.16	0.63	0.63	0.63	0.079 ± 0.017	0.40 ± 0.09
0.62	0.047 ± 0.011	0.063 ± 0.015	4.64 ± 0.21	0.63	0.63	0.63	0.060 ± 0.014	0.28 ± 0.07
0.87	0.044 ± 0.009	0.068 ± 0.014	3.37 ± 0.10	0.62	0.63	0.61	0.066 ± 0.014	0.22 ± 0.05
0.87	0.060 ± 0.014	0.093 ± 0.022	4.98 ± 0.15	0.62	0.63	0.61	0.090 ± 0.021	0.45 ± 0.11
0.88	0.048 ± 0.010	0.074 ± 0.015	4.24 ± 0.13	0.62	0.63	0.61	0.072 ± 0.015	0.30 ± 0.06
0.88	0.041 ± 0.008	0.064 ± 0.012	2.55 ± 0.08	0.62	0.63	0.61	0.062 ± 0.012	0.16 ± 0.03
1.06	0.159 ± 0.050	0.249 ± 0.078	2.53 ± 0.24	0.63	0.63	0.61	0.237 ± 0.074	0.60 ± 0.20
1.08	0.083 ± 0.023	0.132 ± 0.037	2.71 ± 0.26	0.63	0.63	0.61	0.126 ± 0.035	0.34 ± 0.10
1.08	0.088 ± 0.009	0.140 ± 0.014	3.14 ± 0.30	0.63	0.63	0.61	0.133 ± 0.013	0.42 ± 0.06
1.09	0.061 ± 0.015	0.098 ± 0.024	3.30 ± 0.32	0.63	0.63	0.61	0.093 ± 0.023	0.31 ± 0.08
de Ravel et al. 2009; $R_{proj} < 100$ kpc h^{-1}; $1 < L_{primary}/L_{satellite} < 4$; $\delta V < 500$ km s^{-1}; $M_B < -18.77 - 1.11z$								
0.54	$\cdots$	0.22 ± 0.06	$5.27^{+0.92}_{-0.86}$	1.61	1.52	1.54	0.082 ± 0.021	0.43 ± 0.13
0.72	$\cdots$	0.41 ± 0.07	$6.13^{+0.78}_{-0.76}$	1.60	1.50	1.56	0.153 ± 0.027	0.94 ± 0.20
0.90	$\cdots$	0.46 ± 0.07	$5.37^{+1.05}_{-0.99}$	1.62	1.48	1.58	0.169 ± 0.027	0.91 ± 0.23
Kartaltepe et al. 2007; $5 < R_{proj} < 20$ kpc h^{-1}; $\delta z < 0.05$; $M_V < -19.8 - 1.0z$								
0.25	$\cdots$	0.032 ± 0.004	$4.42^{+0.84}_{-0.78}$	0.34	0.34	0.35	0.056 ± 0.007	$0.25^{+0.06}_{-0.05}$
0.35	$\cdots$	0.055 ± 0.003	$4.42^{+0.84}_{-0.78}$	0.35	0.35	0.34	0.094 ± 0.005	0.42 ± 0.08
0.45	$\cdots$	0.039 ± 0.003	$3.53^{+0.78}_{-0.72}$	0.34	0.35	0.34	0.069 ± 0.005	$0.24^{+0.06}_{-0.05}$
0.55	$\cdots$	0.044 ± 0.003	$3.53^{+0.78}_{-0.72}$	0.34	0.35	0.34	0.078 ± 0.005	0.27 ± 0.06
0.65	$\cdots$	0.043 ± 0.002	$3.68^{+0.60}_{-0.56}$	0.33	0.35	0.33	0.078 ± 0.004	0.29 ± 0.05
0.75	$\cdots$	0.049 ± 0.002	$3.68^{+0.60}_{-0.56}$	0.33	0.35	0.33	0.089 ± 0.004	$0.33^{+0.06}_{-0.05}$
0.85	$\cdots$	0.047 ± 0.003	$3.20^{+0.84}_{-0.75}$	0.32	0.35	0.33	0.088 ± 0.006	$0.28^{+0.08}_{-0.07}$
0.95	$\cdots$	0.069 ± 0.003	$3.20^{+0.84}_{-0.75}$	0.32	0.35	0.32	0.129 ± 0.006	$0.41^{+0.11}_{-0.10}$
1.05	$\cdots$	0.071 ± 0.003	$2.65^{+1.65}_{-2.04}$	0.32	0.35	0.32	0.133 ± 0.006	$0.35^{+0.22}_{-0.27}$
1.15	$\cdots$	0.105 ± 0.004	$2.65^{+1.65}_{-2.04}$	0.31	0.35	0.31	0.203 ± 0.008	$0.54^{+0.34}_{-0.42}$
Kartaltepe et al. 2007; $5 < R_{proj} < 20$ kpc h^{-1}; $\delta z < 0.05$; $M_V < -19.8$								
0.15	$\cdots$	0.021 ± 0.007	$5.336^{+0.941}_{-0.828}$	0.34	0.34	0.35	0.04 ± 0.01	$0.20^{+0.07}_{-0.07}$
0.25	$\cdots$	0.018 ± 0.004	$5.543^{+1.049}_{-0.980}$	0.34	0.34	0.35	0.03 ± 0.01	$0.18^{+0.05}_{-0.05}$
0.35	$\cdots$	0.040 ± 0.004	$5.543^{+1.049}_{-0.980}$	0.35	0.35	0.34	0.07 ± 0.01	$0.38^{+0.08}_{-0.08}$
0.45	$\cdots$	0.030 ± 0.003	$5.040^{+1.111}_{-1.024}$	0.34	0.35	0.34	0.05 ± 0.01	$0.27^{+0.06}_{-0.06}$
0.55	$\cdots$	0.034 ± 0.003	$5.040^{+1.111}_{-1.024}$	0.34	0.35	0.34	0.06 ± 0.01	$0.30^{+0.07}_{-0.07}$
0.65	$\cdots$	0.033 ± 0.002	$6.321^{+1.035}_{-0.966}$	0.33	0.35	0.33	0.06 ± 0.00	$0.38^{+0.07}_{-0.06}$
0.75	$\cdots$	0.044 ± 0.002	$6.321^{+1.035}_{-0.966}$	0.33	0.35	0.33	0.08 ± 0.00	$0.51^{+0.09}_{-0.08}$
0.85	$\cdots$	0.045 ± 0.003	$6.575^{+1.726}_{-1.547}$	0.32	0.35	0.33	0.08 ± 0.01	$0.55^{+0.15}_{-0.14}$
0.95	$\cdots$	0.066 ± 0.003	$6.575^{+1.726}_{-1.547}$	0.32	0.35	0.32	0.12 ± 0.01	$0.81^{+0.22}_{-0.19}$
1.05	$\cdots$	0.066 ± 0.003	$7.390^{+4.613}_{-5.688}$	0.32	0.35	0.32	0.12 ± 0.01	$0.91^{+0.57}_{-0.71}$
1.15	$\cdots$	0.102 ± 0.004	$7.390^{+4.613}_{-5.688}$	0.31	0.35	0.31	0.20 ± 0.01	$1.46^{+0.91}_{-1.12}$
				Stellar-mass selected pairs				
de Ravel et al. 2009; $R_{proj} < 100$ kpc h^{-1}; $1 < M_{primary}/M_{satellite} < 4$; $\delta V < 500$ km s^{-1}; $\log[M_{star}] > 10 - 0.187z$								
0.52	$\cdots$	0.14 ± 0.06	$4.11^{+0.61}_{-0.54}$	1.61	1.52	1.54	0.052 ± 0.023	0.21 ± 0.10
0.70	$\cdots$	0.26 ± 0.06	$3.83^{+0.56}_{-0.65}$	1.60	1.50	1.56	0.098 ± 0.022	0.37 ± 0.10
0.90	$\cdots$	0.25 ± 0.06	$3.62^{+0.55}_{-0.59}$	1.62	1.48	1.58	0.093 ± 0.023	0.34 ± 0.10
Bundy et al. 2009; $5 < R_{proj} < 20$ kpc h^{-1}; $1 < M_{primary}/M_{satellite} < 4$; $\delta z < 0.08(1 + z)$; $M_{star} > 10^{10} M_\odot$								
0.55	$\cdots$	0.03 ± 0.02	4.22 ± 0.70	0.33	0.35	0.34	0.055 ± 0.036	0.23 ± 0.16
0.80	$\cdots$	0.05 ± 0.03	4.71 ± 0.60	0.33	0.35	0.33	0.091 ± 0.055	0.43 ± 0.26
1.15	$\cdots$	0.06 ± 0.02	1.56 ± 0.15	0.31	0.35	0.31	0.116 ± 0.039	0.18 ± 0.06

[a] $\Re_{merg}$ and Γ_{merg} are calculated using Equations 3 and 6, and $\langle T_{obs}(z)\rangle_{S08}$. We assume $C_{merge} = 0.6$ for all close pair samples.
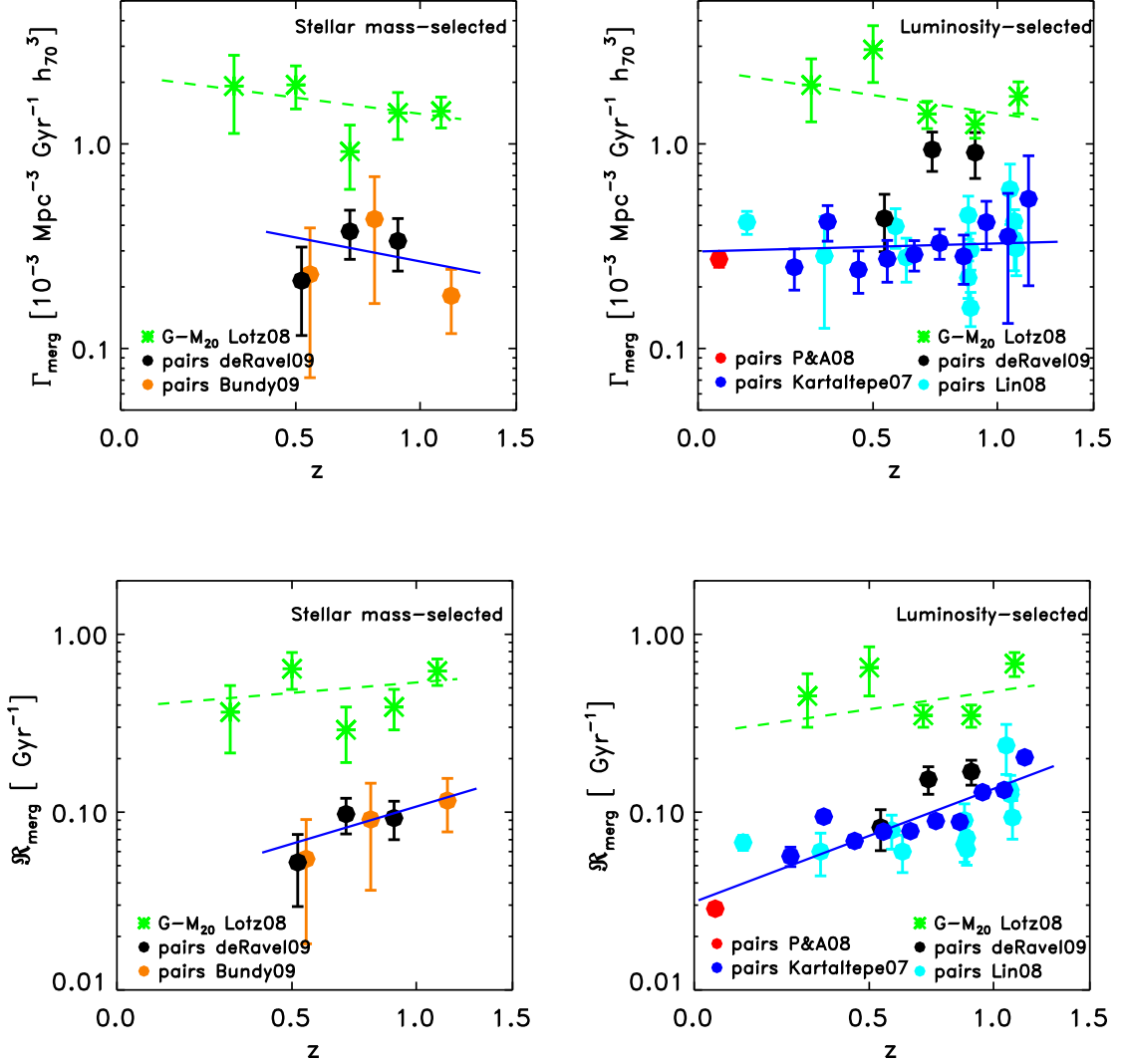
FIG. 10.— Top: Γ_{merg}, the merger rate per co-moving unit volume, for close pairs (circles) and $G - M_{20}$ (asterisks), for stellar mass-selected (left) and rest-frame luminosity selected samples. Bottom: $\Re_{merg}$, the fractional merger rate, for close pairs (circles) and $G - M_{20}$ (asterisks), for the same samples. The error-bars are computed using the observational uncertainties on f_{merg}, f_{pair}, and n_{gal} and do not include uncertainties in $\langle T_{obs} \rangle$. $G - M_{20}$ probes both major and minor mergers, and therefore captures a 'total' merger rate, which is several times higher than the major merger rate probed by these close pair studies. The evolution in $\Gamma_{pairs}(z)$ is weaker than in $\Re_{pairs}(z)$ because f_{pairs} increases with redshift (Fig. 1) while the corresponding n_{gal} decreases with redshift for fixed stellar mass and PLE galaxy selections (Fig. 2). The best-fit slopes for the close pair (major) merger rates (blue solid lines) are given in §5.1 and the best-slopes for the $G - M_{20}$ (total) merger rates (green dashed lines) are given in §5.2.

TABLE 2
$G - M_{20}$ Merger Fractions and Merger Rates

z	f_{merg}	n_{gal} $[10^{-3}\ \mathrm{Mpc}^{-3}]$	$\langle T_{obs}\rangle_{S08}$ [Gyr]	$\langle T_{obs}\rangle_{C06}$ [Gyr]	$\langle T_{obs}\rangle_{St09}$ [Gyr]	$\Re_{merg}$[a] Gyr^{-1}	Γ_{merg}[a] $[10^{-3}\ \mathrm{Gyr}^{-1}\ \mathrm{Mpc}^{-3}]$
Lotz et al. 2008; $M_B \leq -18.94 - 1.3z$							
0.3	0.09 ± 0.03	$4.32^{+0.30}_{-0.27}$	0.20	0.22	0.22	0.45 ± 0.15	1.94 ± 0.66
0.5	0.13 ± 0.04	$4.44^{+0.14}_{-0.15}$	0.20	0.21	0.22	0.65 ± 0.20	2.89 ± 0.89
0.7	0.07 ± 0.01	$4.00^{+0.21}_{-0.18}$	0.20	0.21	0.22	0.35 ± 0.05	1.40 ± 0.21
0.9	0.07 ± 0.01	$3.56^{+0.10}_{-0.12}$	0.20	0.21	0.23	0.35 ± 0.05	1.25 ± 0.18
1.1	0.13 ± 0.02	$2.49^{+0.22}_{-0.26}$	0.19	0.21	0.23	0.68 ± 0.11	$1.70^{+0.30}_{-0.32}$
Lotz et al. 2008; $M_{star} \geq 10^{10} M_\odot$							
0.3	0.07 ± 0.03	5.25 ± 0.24	0.20	0.21	0.22	0.37 ± 0.15	1.84 ± 0.79
0.5	0.13 ± 0.03	3.04 ± 0.12	0.20	0.21	0.22	0.64 ± 0.15	1.98 ± 0.46
0.7	0.06 ± 0.02	3.16 ± 0.11	0.20	0.21	0.22	0.29 ± 0.10	0.95 ± 0.32
0.9	0.08 ± 0.02	3.63 ± 0.09	0.20	0.21	0.23	0.39 ± 0.10	1.45 ± 0.36
1.1	0.12 ± 0.02	2.33 ± 0.07	0.19	0.21	0.23	0.62 ± 0.11	1.47 ± 0.25
$M_B < -19.2$ ($n_{gal} \sim 6 \times 10^{-3} Mpc^{-3}$)							
0.3	0.10 ± 0.02	$4.77^{+0.33}_{-0.29}$	0.20	0.21	0.22	0.52 ± 0.10	$2.48^{+0.51}_{-0.50}$
0.5	0.13 ± 0.02	$6.01^{+0.19}_{-0.20}$	0.20	0.21	0.22	0.66 ± 0.08	$3.97^{+0.50}_{-0.50}$
0.7	0.08 ± 0.01	$6.40^{+0.34}_{-0.28}$	0.20	0.21	0.22	0.41 ± 0.04	$2.59^{+0.29}_{-0.28}$
0.9	0.09 ± 0.01	$7.34^{+0.20}_{-0.25}$	0.20	0.21	0.23	0.47 ± 0.04	$3.41^{+0.31}_{-0.32}$
1.1	0.12 ± 0.01	$6.25^{+0.55}_{-0.66}$	0.19	0.21	0.23	0.61 ± 0.05	$3.78^{+0.47}_{-0.52}$

[a] $\Re_{merg}$ and Γ_{merg} are calculated using Equations 3 and 6, and $\langle T_{obs}(z)\rangle_{S08}$.

TABLE 3
Asymmetry Merger Fractions and Merger Rates

z	f_{merg}	n_{gal} $[10^{-3}\ \mathrm{Mpc}^{-3}]$	$\langle T_{obs}\rangle_{S08}$[a] [Gyr]	$\langle T_{obs}\rangle_{C06}$[a] [Gyr]	$\langle T_{obs}\rangle_{St09}$[a] [Gyr]	$\Re_{merg,S08}$[b] $[\mathrm{Gyr}^{-1}]$	$\Gamma_{merg,S08}$[b] $[10^{-3}\ \mathrm{Gyr}^{-1}\ \mathrm{Mpc}^{-3}]$
Conselice et al. 2009; $M_{star} \geq 10^{10} M_\odot$							
0.25	0.04 ± 0.01	5.25 ± 0.24	0.39/0.46	0.17/0.27	0.24/0.30	0.10 ± 0.03 /0.09 ± 0.02	0.54 ± 0.14/ 0.46 ± 0.12
0.35	0.04 ± 0.01	5.25 ± 0.24	0.41/0.47	0.17/0.27	0.28/0.33	0.10 ± 0.02 /0.09 ± 0.02	0.51 ± 0.13 /0.45 ± 0.11
0.45	0.04 ± 0.01	3.04 ± 0.12	0.45/0.50	0.18/0.28	0.28/0.33	0.09 ± 0.02/ 0.08 ± 0.02	0.27 ± 0.07/ 0.24 ± 0.06
0.55	0.04 ± 0.01	3.04 ± 0.12	0.47/0.52	0.18/0.28	0.31/0.35	0.09 ± 0.02/ 0.08 ± 0.02	0.26 ± 0.07 /0.23 ± 0.06
0.65	0.09 ± 0.01	3.16 ± 0.11	0.53/0.57	0.19/0.28	0.34/0.38	0.17 ± 0.02/ 0.16 ± 0.02	0.54 ± 0.06 /0.50 ± 0.06
0.75	0.12 ± 0.01	3.16 ± 0.11	0.53/0.56	0.20/0.29	0.34/0.38	0.23 ± 0.02/ 0.21 ± 0.02	0.72 ± 0.06 /0.68 ± 0.06
0.85	0.11 ± 0.01	3.63 ± 0.09	0.62/0.64	0.21/0.30	0.35/0.38	0.18 ± 0.02 /0.17 ± 0.02	0.64 ± 0.06 /0.62 ± 0.06
0.95	0.10 ± 0.01	3.63 ± 0.09	0.63/0.64	0.21/0.30	0.38/0.41	0.16 ± 0.02/ 0.16 ± 0.02	0.58 ± 0.06 /0.57 ± 0.06
1.05	0.11 ± 0.01	2.33 ± 0.07	0.68/0.69	0.22/0.31	0.38/0.41	0.16 ± 0.01 /0.16 ± 0.01	0.38 ± 0.04/ 0.37 ± 0.04
1.15	0.13 ± 0.01	2.33 ± 0.07	0.70/0.71	0.23/0.31	0.44/0.47	0.19 ± 0.01/ 0.18 ± 0.01	0.43 ± 0.04/ 0.43 ± 0.04
López-Sanjuan et al. 2009; $M_{star} \geq 10^{10} M_\odot$							
0.4	0.006 ± 0.02	4.22 ± 0.70	0.43/0.49	0.17/0.27	0.27/0.33	0.01 ± 0.05 /0.01 ± 0.04	$0.15^{+0.49}_{-0.49}$/ $0.09^{+0.31}_{-0.31}$
0.725	0.022 ± 0.01	4.71 ± 0.60	0.54/0.58	0.19/0.29	0.34/0.38	0.04 ± 0.02/ 0.04 ± 0.02	$0.54^{+0.25}_{-0.25}$/ $0.36^{+0.17}_{-0.17}$
0.975	0.037 ± 0.01	1.56 ± 0.15	0.65/0.67	0.21/0.30	0.37/0.40	0.06 ± 0.02/ 0.06 ± 0.01	$0.27^{+0.08}_{-0.08}$/ $0.19^{+0.05}_{-0.05}$
Shi et al. 2009; $M_B \leq -18.94 - 1.3z$							
0.3	0.21 ± 0.04	$4.32^{+0.30}_{-0.27}$	0.40/0.47	0.17/0.26	0.26/0.32	0.52 ± 0.10/ 0.45 ± 0.09	$2.27^{+0.46}_{-0.45}$ /$1.93^{+0.39}_{-0.39}$
0.5	0.24 ± 0.03	$4.44^{+0.14}_{-0.15}$	0.46/0.51	0.18/0.27	0.29/0.34	0.52 ± 0.07/ 0.47 ± 0.06	$2.32^{+0.30}_{-0.30}$ /$2.09^{+0.27}_{-0.27}$
0.7	0.25 ± 0.02	$4.00^{+0.21}_{-0.18}$	0.53/0.56	0.19/0.29	0.34/0.38	0.47 ± 0.04/ 0.45 ± 0.04	$1.89^{+0.18}_{-0.17}$ /$1.79^{+0.17}_{-0.16}$
0.9	0.36 ± 0.03	$3.56^{+0.10}_{-0.12}$	0.62/0.64	0.21/0.30	0.36/0.40	0.58 ± 0.05/ 0.56 ± 0.05	$2.07^{+0.18}_{-0.19}$ /$2.00^{+0.18}_{-0.18}$
1.1	0.30 ± 0.03	$2.49^{+0.22}_{-0.26}$	0.69/0.70	0.23/0.32	0.41/0.44	0.43 ± 0.04/ 0.43 ± 0.04	$1.08^{+0.14}_{-0.16}$ /$1.07^{+0.14}_{-0.15}$

[a] $\langle T_{obs}\rangle$ calculated assuming both $T_{obs}(A) = 0$ for $f_{gas} < 0.1$, and $T_{obs}(A)$ at $f_{gas} < 0.1$ is the same as $T_{obs}(A)$ at $f_{gas} \sim 0.2$.
[b] $\Re_{merg}$ and Γ_{merg} are calculated using Equations 3 and 6, and $\langle T_{obs}(z)\rangle_{S08}$.

left panel) are given in Table 4.

On the right hand side of Figure 10, we plot Γ and $\Re$ for close pairs selected with evolving luminosity cuts from Lin et al. 2008 (cyan circles), de Ravel et al. 2009 (black circles), and Kartaltepe et al. 2007 (blue circles), and the $z \sim 0.1$ value from the Patton & Atfield 2008 study (red circle). Most of these studies give very consistent galaxy merger rates once corrected for the observability timescales, although the de Ravel et al (2009) luminosity-selected bright pairs have a merger rate ~ 3 times higher than the other studies at $z \sim 0.7 - 1$. However, the number density of galaxies with the passive luminosity evolution (PLE) assumptions adopted by de Ravel et al. (2009) is also $\sim 2 - 3$ times higher than the selection adopted by the other studies. As we discuss in §5.4, the de Ravel et al. (2009) luminosity-selected pairs are in good agreement with other studies selected at similar number densities. We exclude the de Ravel et al. (2009) pairs and give the best fit volume-averaged merger rate for the luminosity-selected close pairs $\Gamma_{pairs,PLE}(z)$ (blue line, top right panel) and fractional merger rate $\Re_{pairs,PLE}(z)$ (blue line, bottom right panel) in Table 4.

5.2. $G - M_{20}$ and the Minor Merger Rate

We also calculate Γ and $\Re$ from the $G - M_{20}$ merger fractions for the stellar-mass and evolving luminosity selected parent samples (Table 2; green points in Figure 10). Both $\Gamma_{G-M_{20}}$ and $\Re_{G-M_{20}}$ are significantly higher than the merger rates calculated for close pairs. The best-fit evolution with redshift in the $G - M_{20}$ merger rates is systematically weaker than that for the close pairs, but have slopes that are consistent within the large uncertainties. As we discussed in §4, $G - M_{20}$ is sensitive to mergers with baryonic mass ratios between 1:1 and 1:10, while the close pair studies plotted in Figure 10 have mass ratios 1:1 - 1:4. Therefore the $G - M_{20}$ merger rate includes minor as well as major mergers, and is expected to be significantly higher than the major merger rate.

We give the best-fit $G - M_{20}$-derived volume-averaged 'total' merger rate $\Gamma_{G-M_{20}}$ and 'total' merger rate per galaxy $\Re_{G-M_{20}}$ for stellar mass selected and luminosity-selected parent samples in Table 4 and Figure 10 (green dashed lines). The $G - M_{20}$ merger rates evolve weakly with redshift, and show trends consistent with the pair merger rate evolution within the large uncertainties. However, the $G - M_{20}$ merger rates are much higher than the corresponding close pair merger rates at $z \sim 0.7$, where the merger rates are best determined. We can estimate the minor merger rate for galaxies with mass ratio between 1:4 and 1:10 by subtracting the best-fit close-pair derived major merger rate from the total $G - M_{20}$ merger rate. These minor merger rates are given in Table 4.

We find that the fractional and volume-averaged minor merger rate at $z \sim 0.7$ is ~ 3 times that of the major merger rate for galaxies selected by stellar mass or PLE. This ratio does not evolve significantly with redshift between $0.2 < z < 1.2$. Our findings are roughly consistent with the relative numbers of minor/major mergers from the visual classification study of Jogee et al. (2009), who find ~ 3 minor mergers for every major merger for galaxies selected at $0.24 < z < 0.8$ and $M_{star} > 2.5 \times 10^{10} M_{\odot}$. However, the absolute value of the major+minor merger

rate per co-moving volume (Γ) calculated in Jogee et al. (2009) is a factor of ten lower than what we find here, in part because of the higher mass limit of their sample. Weaker evolution of minor mergers relative to major mergers is also seen in the close pair study at $z < 1$ by López-Sanjuan et al. (2011). In this case, however, López-Sanjuan et al. (2011) find only $0.5 - 1$ minor merger pairs (with rest-frame B-band luminosity ratios between 1:10 and 1:4) per major merger pair. Finally, we note that our estimates of the minor merger rate are contingent upon the accuracy of both our close-pair determined major merger rate and $G - M_{20}$ determined 'total' merger rates.

5.3. Asymmetry Merger Rates

Both observational and theoretical uncertainties make it difficult to calculate the merger rate reliably with asymmetric galaxies. The asymmetric fraction measured by three different groups for the same data vary by a factor of ten, reflecting different corrections for surface-brightness dimming and contamination by non-mergers. Furthermore, the timescales needed to compute merger rates also vary by factors of 2-3, depending on the assumed distribution and evolution of gas fractions. The high-resolution merger simulations predict that asymmetry is sensitive to mergers with mass ratios less than 1:4 for local gas fractions, and 1:10 for high gas fractions. Therefore, in order to be consistent with the results from close pairs and $G - M_{20}$ mergers, the merger rate from asymmetry should lie between the close pair derived major merger rate and the $G - M_{20}$ major + minor merger rate.

We calculate $\Gamma_A(z)$ and $\Re_A(z)$ (Table 3, Figure 11), using the asymmetric galaxy fraction measurements from Conselice et al. 2009 (left panel), López-Sanjuan et al. 2009 (center panel), and Shi et al. 2009 (left panel) and $\langle T_{obs}(A, z) \rangle$ predicted by the S08 (black points), C06 (blue points), and St09 (red points) models from Figure 9. The uncertainty in $\langle T_{obs}(A) \rangle$ results in a factor of 2-3 uncertainty in Γ and $\Re$ for a given set of asymmetry measurements. For a given $\langle T_{obs}(A) \rangle$, the calculated Γ_A and $\Re_A$ vary by a factor of ten for the different asymmetry studies. The volume-averaged asymmetry-derived merger rates Γ_A have weak evolution with redshift, with best-fit α values ranging from -1 to $+0.4$. The fractional asymmetry-derived merger rates $\Re_A$ evolve more strongly with redshift, with best-fit m values ranging from $+0.1$ to $+1.6$. (We exclude the fits to the López-Sanjuan et al. points because of their large uncertainties.)

We compare the asymmetry-derived merger rates to the close pair major merger (blue solid lines) and $G - M_{20}$ major+minor merger rates (green dashed lines) computed for parent samples with similar selections. If the distribution of merger properties predicted by the S08 models is correct, then asymmetry should select many gas-rich minor mergers and be expected to give $\Gamma_A(z)$ and $\Re_A(z)$ similar to those calculated with $G - M_{20}$ (green dashed lines). We find this to be the case for the Shi et al. observations (black diamonds, right panels), while the Conselice et al. observations and López-Sanjuan et al. observations with S08 timescales give merger rates significantly lower than the $G - M_{20}$ merger rate (black diamonds, left and center panels). On the
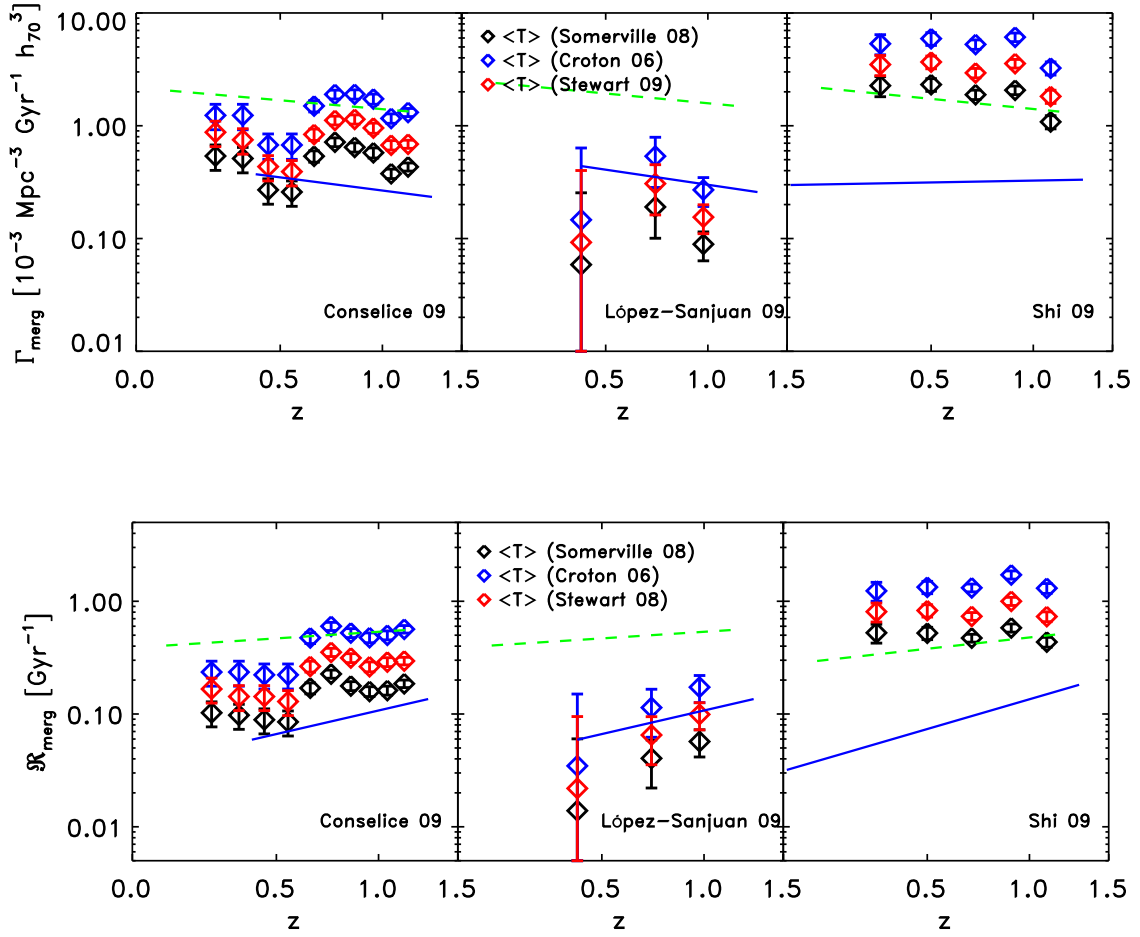
Fig. 11.— Top: Γ_{merg}, the merger rate per co-moving unit volume for asymmetric galaxies, for Conselice et al. 2009 and López-Sanjuan et al. 2009 stellar mass-selected samples (left, center) and the Shi et al. 2009 rest-frame B luminosity selected sample (right). Bottom: $\Re_{merg}$, the fractional merger rate for the same samples. Γ_{merg} and $\Re_{merg}$ are calculated using the three different observability timescales (Somerville et al. 2008, black; Croton et al. 2006, blue; Stewart et al. 2009b, red) for each study. For comparison are the best-fit to the major merger rates from the close pairs (blue solid lines) and major+minor merger rates from $G - M_{20}$ (green dashed lines) from Figure 10. The error-bars are computed using the observational uncertainties on f_{merg} and n_{gal} and do not include uncertainties in $\langle T_{obs} \rangle$.

other hand, if most mergers have low gas fractions at $z \sim 1$ (C06), then $\Gamma_A(z)$ and $\Re_A(z)$ are expected to probe 1:1 - 1:4 mass ratio mergers and be consistent with the close pair major merger rate (blue solid lines). The López Sanjuan et al. observations + C06 timescales are roughly consistent with the close-pair major merger rates (blue diamonds, center panels). Finally, if the intermediate gas-evolution scenario of St09 is correct, then asymmetric galaxies are more likely to be mergers with intermediate mass ratios between 1:4 and 1:10, as suggested by the Conselice et al. observations + St09 timescales (red diamonds, left panels). Until better observational constraints on the distribution and evolution in f_{gas} are available, we cannot determine if (or which) asymmetry merger rate calculations are in agreement with other methods for measuring the galaxy merger rate.

5.4. Merger Rates for galaxies at constant $n_{gal}(z)$

As we discussed in §3.5, the derived evolution in the galaxy merger rate depends in large part on which galaxies are included in the sample. It is clear from Fig-

ure 2 that selecting galaxy samples above a fixed stellar mass or with a PLE assumption does not track the same progenitor-descendant populations. A better (although still not perfect) way to track the same population of galaxies (and dark matter halos) with redshift is to select galaxies above a fixed number density. No galaxy merger studies published to date have been designed to use a constant number density selection. However, we find that the fixed rest-frame V luminosity cut employed by Kartaltepe et al. (2007) close pair study results in a roughly constant number density selection (Figure 12, left). Kartaltepe et al. (2007) selected their parent sample above a fixed absolute luminosity for $0.1 < z < 1.2$, arguing that galaxy pairs and mergers would not follow a simple passive luminosity evolution because of merger-induced star-formation. The luminosity cut adopted by de Ravel et al. $(M_B < -18.77 + 1.1z)$ also selects a roughly constant and similar number density of galaxies (black points). In order to compare the $G - M_{20}$ results to these studies, we adopt a fixed rest-frame B luminosity cut of $M_B(AB) < -19.2$ which selects galaxies at a simi-
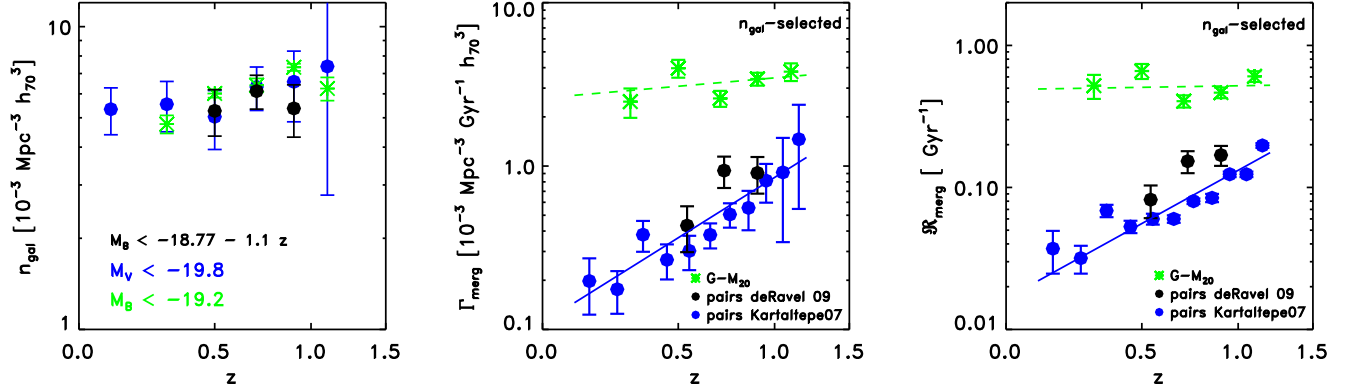
FIG. 12.— Left: The Kartaltepe et al. (2007; blue points) and de Ravel et al. (2009; black points) parent galaxy selections result in a sample of galaxies with roughly constant n_{gal} from $0.1 < z < 1.2$. For comparison, we select $G - M_{20}$ merger candidates with a fixed M_B limit ≤ -19.2 (green asterisks) in order to match the roughly constant n_{gal} of these studies. Center: The galaxy merger rates per unit co-moving volume for samples selected at constant n_{gal} v. redshift. . Right: The galaxy merger rates per galaxy for samples selected at constant n_{gal} v. redshift. We find strong evolution in $\Gamma_{pairs,n_{gal}}$ and $\Re_{pairs,n_{gal}} \propto (1+z)^3$, and weaker evolution in the 'total' and inferred minor merger rates (see Table 4). The error-bars are computed using the observational uncertainties on f_{merg}, f_{pair}, and n_{gal} and do not include uncertainties in $\langle T_{obs} \rangle$.

TABLE 4
MAJOR AND MINOR GALAXY MERGER RATES AT $z < 1.5$

Selection	Mass Ratio	$C \times (1+z)^{\alpha}$
Volume-Averaged Total Merger Rates [10^{-3} Gyr^{-1} Mpc^{-3} h$_{70}^3$]		
$\Gamma_{G-M_{20},M_{star}}(z)$	1:1 - 1:10 (30)	$(2.2 \pm 2.7)(1+z)^{-0.6 \pm 1.6}$
$\Gamma_{G-M_{20},PLE}(z)$	...	$(2.3 \pm 2.5)(1+z)^{-0.7 \pm 1.5}$
$\Gamma_{G-M_{20},n_{gal}}(z)$	...	$(2.60 \pm 0.06)(1+z)^{+0.4 \pm 0.9}$
Total Merger Rates per galaxy [Gyr^{-1}]		
$\Re_{G-M_{20},M_{star}}(z)$	1:1 - 1:10 (30)	$(0.4 \pm 0.4)(1+z)^{+0.5 \pm 1.6}$
$\Re_{G-M_{20},PLE}(z)$	...	$(0.3 \pm 0.2)(1+z)^{+0.8 \pm 1.4}$
$\Re_{G-M_{20},n_{gal}}(z)$	...	$(0.5 \pm 0.3)(1+z)^{+0.1 \pm 0.8}$
Volume-Averaged Major Merger Rates [10^{-3} Gyr^{-1} Mpc^{-3} h$_{70}^3$]		
$\Gamma_{pairs,M_{star}}(z)$	1:1 - 1:4	$(0.5 \pm 1.4)(1+z)^{-0.9 \pm 3.2}$
$\Gamma_{pairs,PLE}(z)$	...	$(0.30 \pm 0.04)(1+z)^{+0.1 \pm 0.4}$
$\Gamma_{pairs,n_{gal}}(z)$	...	$(0.11 \pm 0.03)(1+z)^{+3.0 \pm 1.1}$
Major Merger Rates per galaxy [Gyr^{-1}]		
$\Re_{pairs,M_{star}}(z)$	1:1 - 1:4	$(0.03 \pm 0.01)(1+z)^{+1.7 \pm 1.3}$
$\Re_{pairs,PLE}(z)$	...	$(0.03 \pm 0.01)(1+z)^{+2.11 \pm 0.2}$
$\Re_{pairs,n_{gal}}(z)$	...	$(0.016 \pm 0.001)(1+z)^{+3.0 \pm 0.3}$
Volume-Averaged Minor Merger Rates [10^{-3} Gyr^{-1} Mpc^{-3} h$_{70}^3$]		
$\Gamma_{minor,M_{star}}(z)$	1:4 - 1:10 (30)	$(0.8 \pm 5.1)(1+z)^{-0.2 \pm 2.8}$
$\Gamma_{minor,PLE}(z)$	...	$(1.0 \pm 0.1)(1+z)^{-0.3 \pm 1.0}$
$\Gamma_{minor,n_{gal}}(z)$	...	$(2.6 \pm 1.1)(1+z)^{+0.1 \pm 1.6}$
Minor Merger Rates per galaxy [Gyr^{-1}]		
$\Re_{minor,M_{star}}(z)$	1:4 - 1:10 (30)	$(0.27 \pm 0.08)(1+z)^{-0.1 \pm 0.7}$
$\Re_{minor,PLE}(z)$	...	$(0.28 \pm 0.08)(1+z)^{-0.1 \pm 0.6}$
$\Re_{minor,n_{gal}}(z)$	...	$(0.37 \pm 0.03)(1+z)^{-0.2 \pm 0.2}$

The lower limit of the baryonic mass ratio for $G - M_{20}$ detected mergers is between 1:10 and 1:30. See §5 for discussion.

lar number density at each redshift bin (Figure 12, left). We compute the $G - M_{20}$ fraction and merger rates for galaxies selected at $M_B(AB) < -19.2$ (Table 2, Figure 12).

When a roughly constant co-moving number density ($n_{gal} \sim 6 \times 10^{-3}$ Mpc^{-3}) selection is applied to the parent sample, the close-pair derived galaxy merger rates show strong evolution with redshift, as concluded by Kartaltepe et al. (2007). Combining the Kartaltepe et al. (2007) and de Ravel et al. (2009) samples (Table 1), we find the galaxy merger rate per unit co-moving volume $\Gamma_{pairs,n_{gal}}$ (blue line, center panel) evolves much more strongly ($\alpha = +3.0 \pm 1.1$) than than the merger rate derived for the PLE parent sample with a declining number density ($\alpha = +0.1 \pm 0.4$; see Table 4). The evolution in fractional merger rate $\Re_{pairs,n_{gal}}$ is similar to the evolution in volume-averaged merger rate. The best-fit to the $G - M_{20}$ major+minor rates for galaxies selected by number density have systematically weaker evolution (although the uncertainties are large). At $z \sim 0.7$, the volume-averaged and fractional minor merger rates for galaxies selected at $n_{gal} \sim 6 \times 10^{-3}$ Mpc^{-3} are $\sim 4 - 5$ times the major merger rates (Table 4).

5.5. Theoretical Predictions for Major and Minor Galaxy Merger Rates

We compare the theoretical predictions for the galaxy merger rates to the major and major+minor merger rates for the stellar-mass selected samples in Figure 13. Because we have used only the *relative* distribution of merger properties from the S08, St09, and C06 models to calculated $\langle T_{obs}(z) \rangle$, the predictions of the volume-averaged and fractional merger rates from those models are independent of our timescale calculations. We do incorporate the relative numbers of minor and major mergers into our timescale calculations, but in practice only the asymmetry timescales are strongly dependent on the assumed mass ratio distributions. We also compare to the Hopkins et al. (2010b) semi-empirical model predictions using their merger_rate_calculator.pro IDL routine. We calculate the predicted merger rates for galaxies at $0.1 < z < 1.5$ with stellar masses $M_{star} \geq 10^{10} M_{\odot}$ and stellar mass ratios between 1:1-1:4 (solid lines, upper
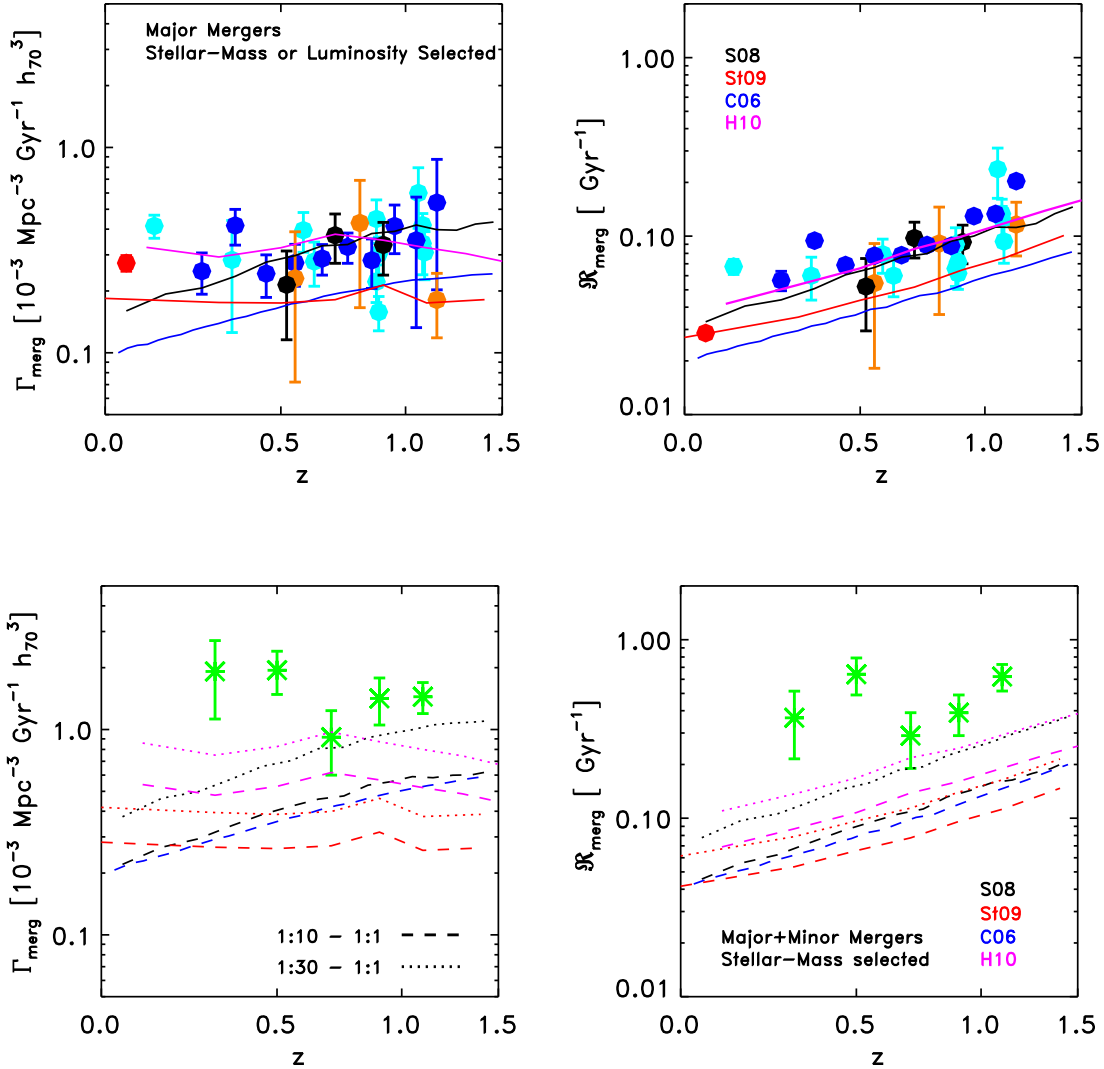
FIG. 13.— Observed Galaxy Merger Rates v. Theoretical Predictions. *Top:* The volume-averaged (top left) and fractional major merger (top right) rates given by stellar-mass and luminosity-selected close pairs are compared to the major merger rates given by the S08 (black lines), St09 (red lines), C06 (blue line), and Hopkins et al. 2010b (magenta lines) models for 1:1 - 1:4 stellar mass ratio mergers and galaxies with $M_{star} > 10^{10} \ M_{\odot}$. The theoretical predictions are in good agreement with the observed major merger rates. *Bottom:* The volume-averaged (bottom left) and fractional major + minor merger (bottom right) rates given by stellar-mass selected $G - M_{20}$ mergers are compared to the major + minor merger rates given by the same models for 1:1 - 1:10 (dashed lines) and 1:1 - 1:30 (dotted lines) stellar mass ratios and galaxies with $M_{star} > 10^{10} \ M_{\odot}$. The observed $G - M_{20}$ 'total' merger rates are an order of magnitude higher than the predicted 1:1-1:10 merger rates, and a factor of 2-3 times higher than the predicted 1:1-1:30 merger rates.

panels in Fig. 13), 1:1-1:10 (dashed lines, lower panels), and 1:1-1:30 (dotted lines, lower panels).

We find that predicted major merger rates agree within a factor of ~ 2 of each other, and are in good agreement with the close pair-derived major merger rates (top panels, Fig. 13). (For completeness, we have also plotted the luminosity-selected close pairs as these give the same merger rate as the stellar-mass selected pairs). The evolution in the volume-averaged major merger rate Γ_{merg} is somewhat weaker and in better agreement with the data for the semi-empirical models (St09, H10). This is likely because those models use $n_{gal}(z)$ as an input parameter rather than give independent predictions for $n_{gal}(z)$ as the S08 and C06 models do. The evolution in

the fractional major merger rate $\Re_{merg}$ is similar for all the models, and in excellent agreement with the data.

On the other hand, the predicted total merger rates (major+minor) are significantly lower than what is observed for $G-M_{20}$ mergers. Given the uncertainty in the lower mass ratio limit for $G-M_{20}$-selected mergers, we show both the 1:1-1:10 and 1:1-1:30 total merger rates. The 1:1-1:10 merger rates are a factor of 5 less than the $G-M_{20}$-derived merger rates, while the 1:1-1:30 merger rates are a factor $\sim$ 2-3 lower. The evolutionary trends with redshift are similar to the major merger predictions, with weaker evolution in Γ_{merg} for the semi-empirical models that follows the same evolutionary trend as the data.

There are several possible reasons for the discrepancy in normalization of the minor merger rates. The $G-M_{20}$ merger rates could be over-estimated, either because it suffers from large contamination of non-merging systems or because we have under-estimated $\langle T_{obs}(z) \rangle$. Alternatively, the models could under-estimate the frequency of minor mergers. A primary galaxy of stellar mass $\sim 10^{10} M_\odot$ undergoing a 1:10 merger will have a merging satellite galaxy with a stellar mass of $\sim 10^9 M_\odot$; a 1:30 merger will have a merging satellite will have a stellar mass of $3 \times 10^8 M_\odot$. The total halo masses are roughly 10 times higher, but are still approaching the numerical resolution of merger trees based on numerical simulations with typical particle masses $\sim 3 \times 10^8 M_\odot$ (e.g. St09, C06, H10). Also, low mass satellite galaxies are strongly effected by difficult-to-model physics, including supernova feedback and satellite disruption. Therefore it is possible that the simulations have incompletely sampled the minor merger populations (e.g. Hopkins et al. 2010a). Both higher resolution models and improved estimates of the minor merger rates are needed to resolve this discrepancy.

6. SUMMARY

We attempt to reconcile the disparate observational estimates of the galaxy merger rate at $z < 1.5$, and calculate the fractional (per galaxy) and volume-averaged (per co-moving volume) galaxy merger rates for major (1:1 - 1:4) and minor (1:4 - 1:10) mergers. When physically-motivated cosmologically-averaged timescales, similar parent sample selections, and consistent definitions of the merger rate are adopted, we are able to derive self-consistent estimates of the major and minor galaxy merger rate and its evolution. We conclude that the differences in the observed galaxy merger fractions may accounted for by the different observability timescales, different mass-ratio sensitivities, and different parent galaxy selections.

We compute the first cosmologically-averaged observability timescales for three different approaches to identifying mergers – close pairs, $G - M_{20}$ and asymmetry – using the results of a large suite of high-resolution N-body/hydrodynamical merger simulations and three different cosmological galaxy evolution models to predict the distribution of galaxy merger mass ratios and baryonic gas fractions. The timescales for close pairs and $G - M_{20}$ are relatively insensitive to the assumptions about the distribution of galaxy merger properties. However, the cosmologically-averaged asymmetry timescales vary by a factor of $2 - 3$ with different assumptions for the distribution and evolution of baryonic gas fractions. In particular, if the mean gas fraction of merging galaxies evolves as strongly as recent observations suggest, then the typical timescale for identifying a galaxy merger via asymmetry may increase by a factor of 2 from $z \sim 0$ to $z \sim 1.5$. We apply these timescales to the close pair fraction and morphologically-determined merger fractions at $z < 1.5$ published in the recent literature to compute merger rates. We estimate the minor merger rate by computing the difference between the close pair-derived and $G - M_{20}$-derived merger rates.

We find the following:

(1) The evolution of the major and minor merger rates of galaxies depends upon the definition of merger rate (fractional or volume-averaged) and the selection of the parent sample of galaxies for which the merger rate is measured. For parent samples of fixed stellar mass or with an assumption of passive luminosity evolution (PLE), the evolution in the volume-averaged merger rate Γ_{merg} [Gyr^{-1} Mpc^{-3}] is significant weaker than the evolution in the fractional merger rate $\Re_{merg}$ [Gyr^{-1}]. This is because the co-moving number density of galaxies with these selections declines by a factor of $2 - 3$ from $z \sim 0$ to $z \sim 1.5$.

(2) The fractional and volume-averaged major merger rates at $0 < z < 1.5$ for galaxies selected above a fixed stellar mass or assuming passive luminosity evolution are calculated for close pairs with stellar mass ratios or optical luminosity ratios between 1:1 and 1:4 (Tables 1 and 4). The number of major mergers per bright/massive galaxies increases as $\sim (1 + z)^2$ with redshift, but the number of major mergers per co-moving volume (selected above a constant stellar mass) does not evolve significantly with redshift. The major merger rates for galaxies selected with $M_{star} \geq 10^{10} M_\odot$ and with $L_B > 0.4 L_B^*$ agree within the uncertainties, implying that luminosity brightening does not strongly bias the (evolving) luminosity-selected sample.

(3) The $G - M_{20}$ derived merger rates for similarly-selected parent samples are significantly larger than the close-pair derived major merger rates (Tables 2 and 4). This is consistent with the simulation predictions that $G - M_{20}$ selected mergers span a wider range of mass ratio (1:1- 1:10) than the close pair major-merger studies (1:1 -1:4). We estimate the minor merger ($1:4 > M_{satellite} : M_{primary} > 1:10$) rate by subtracting the best-fit close pair merger rate from the $G - M_{20}$ merger rate (Table 4). The fractional and volume-averaged minor merger rates are ~ 3 times the major merger rates at $z \sim 0.7$, and suggest weaker evolution in the minor merger rate than the major merger rate at $z < 1$.

(4) The merger rates derived from observations of the fraction of asymmetric galaxies are highly uncertain (Table 3). Different methodologies for correcting asymmetry for surface-brightness dimming, sky noise, and false merger contamination result in a factor of 10 discrepancy in the literature values of the fraction of asymmetric galaxies. The theoretical average observability timescales add a factor of a few uncertainty to the asymmetry merger rate, because of their dependence on the unknown distribution of f_{gas}. The asymmetry-derived merger rates generally fall between the close-pair major merger rates and the $G - M_{20}$ major+minor rates, as expected for the range of predicted merger mass ratios for asymmetric galaxies ($> 1 : 4 - 1 : 10$).

(5) We have also measured the galaxy merger rates for samples selected with roughly constant co-moving number density ($n_{gal}(z) \sim 6 \times 10^{-3}$ Mpc^{-3}). This selection results in stronger evolution in the merger rate, because it probes fainter/less massive galaxies at higher z and brighter/more massive galaxies at low z than fixed stellar mass selection. This selection also is expected to better track progenitor-descendant populations, and better match dark matter halo merger rate calculations. Strong evolution in the major merger rates at roughly constant co-moving number density are observed (Table 4), with $\Gamma_{pairs,n_{gal}}$ and $\Re_{pairs,n_{gal}} \propto (1 + z)^3$. However, the in-

ferred minor merger rates at constant number density evolve weakly with redshift.

(6) The major-merger rates and their evolution with redshift for stellar-mass selected close pairs are in excellent agreement with a number of recent galaxy evolution models (Hopkins et al. 2010b, S08, C06, St09). The 'total' merger rates for stellar-mass selected $G - M_{20}$ mergers is significantly higher than the 1:1 -1:10 and 1:-1:30 stellar-mass ratio merger rates for the same models. It is possible that the $G - M_{20}$ merger rate is over-estimated, or that the models incompletely sample low-mass satellite galaxies and minor mergers. Additional work on both the observational and theoretical fronts is needed to resolve this issue.

REFERENCES

Abraham, R. , Valdes, F., Yee, H.K.C., & van den Bergh, S. 1994, ApJ, 432, 75

Abraham, R. et al. 1996, MNRAS, 279, L47

Abraham R.G., van den Bergh S., & Nair P. 2003, ApJ, 588, 218

Barton, E. J., Arnold J.A., Zentner A.R., Bullock J.S., & Wechsler R.H. 2007, ApJ, 671, 1538

Beckwith, S.V.W. et al. 2006, AJ, 132, 1729

Bell, E.F., McIntosh, D., Katz, N., & Weinberg M.D., 2003, ApJS, 149, 289

Bell, E. F., et al. 2004, 608, 752

Bell, E. F., et al. 2006, ApJ, 640, 241

Benson, A.J. et al. 2003 ApJ, 599, 38

Benson, A.J. 2005, MNRAS, 358, 551

Berrier, J.C., Bullock, J.S., Barton, E., Guenther, H.D., Zentern,A.R., & Wechsler, R.H. 2006, ApJ, 652, 56

Borsch, A., et al. 2006, A&A 453, 869

Bridge, C., Carlberg, R.G., & Sullivan M. 2010, ApJ, 709, 1067

Brown, M.J.I., et al. 2007, ApJ, 654, 858

Bruzual, G. & Charlot, S. 2003, MNRAS, 344, 1000

Bundy K., Fukugita M., Ellis R.S., Kodama T., & Conselice C.J. 2004, ApJ, 601, L123

Bundy, K., Ellis, R.S., & Conselice, C.J. 2005, ApJ, 621

Bundy, K., et al. 2006, ApJ, 651, 120

Bundy, K., Fukugita M, Ellis RS, Targett TA, Belli S, & Kodama T. 2009, ApJ, 697, 1369

Cassata, P., et al. 2005, MNRAS, 357, 903

Chabrier, G., 2003, PASP, 115, 763

Conroy, C. & Wechsler, R.H. 2009, ApJ, 696, 620

Conselice, C.J., Bershady, M.A., & Jangren, A. 2000, AJ, 529, 886

Conselice, C.J., Bershady, M.A., Dickinson, M., & Papovich, C. 2003, AJ, 126, 1183

Conselice, C.J., Blackburne, J.A., & Papovich, C. 2005, ApJ, 620, 564

Conselice, C.J., Yang, C., & Bluck, A.F.L. 2009, MNRAS, 394, 1956

Cox, T.J., Jonsson, P., Primack, J.R., Somerville, R.S. 2006, MNRAS, 373, 1013

Cox, T.J., Jonsson, P., Somerville, R.S., Primack, J.R., & Dekel, A. 2008, MNRAS, 384, 386

Croton, D., et al. 2006, MNRAS, 365, 11 [C06]

Davis, M., et al. 2007, ApJ, 660, L1

Darg, D.W., et al. 2010, MNRAS, 401, 1043

Daddi, E., et al. 2010, ApJ, 713, 686

de Ravel, L., et al. 2009, A&A 498, 379

de Propris R., Liske J., Driver S.P., Allen P.D., & Cross N.J.G. 2005, AJ, 130 1516

Dickinson, M., Papovich, C., Ferguson, H.C., & Budavári, T. 2003,ApJ, 587, 25

Di Matteo T., Colberg J., Springel V., Hernquist L., & Sijacki D. 2008, ApJ, 676, 33

Dory, N., Salvato, M., Gabasch, A., Bender, R., Hopp, U., Feulner, G., & Pannella, M. 2005, ApJ, 619, L131

Erb, D., Steidel, C.C., Shapley, A.E., Pettini, M., & Reddy, N.A.2006, ApJ, 646, 107

Faber, S.M., et al. 2007, ApJ, 665, 265

Fakhouri, O., & Ma, C. 2008, MNRAS, 386, 577

Fakhouri, O., Ma, C., & Boylan-Kolchin, M. 2010, MNRAS, 406, 2267

Fontana, A., et al. 2006, A&A, 459, 745

Fontantot, F., de Lucia, G., Moanco, P., Somerville, R.S., & Santinti, P. 2009, MNRAS, 397, 1776

Genel, S., Genzel, R., Bouché, N., Naab, T., & Sternberg, A. 2009, ApJ, 701, 2002

Giavalisco, M., et al. 2004, ApJ, 600, L93

Gottolöber, S., Klypin, A., & Kravtsov, A.V. 2001, ApJ, 546, 223

Hopkins, A. & Beacom, J.F. 2006, ApJ, 651, 142

Hopkins, P.F., Hernquist, L., Cox, T.J., Di Matteo, T., Robertson, B., & Springel, V. 2006, ApJS, 163, 1

Hopkins, P.F., Hernquist, L., Cox, T.J., & Keres, D. 2008, ApJS, 175, 356

Hopkins, P.F., et al. 2010a, ApJ, 724, 915

Hopkins, P.F., et al. 2010b, ApJ, 715, 202

Hubble, E. 1926, ApJ, 64, 321

Ilbert, O., et al. 2005, A&A, 439, 863

Ilbert, O., et al. 2010, ApJ, 709, 644

Jogee, S., et al. 2009, ApJ, 697, 1971

Jonsson, P., 2006, MNRAS, 372, 2

Jonsson, P., Cox, T.J., Primack, J., & Somerville R. 2006, ApJ, 637, 255

Kartaltepe, J., et al. 2007, ApJS, 172, 320

Kartaltepe, J., et al. 2010, ApJ, 721, 98

Kampczyk, P., et al. 2007, ApJS, 172, 329

Kauffmann, G., White, S.D.M., & Guiderdoni, B. 1993, MNRAS, 264, 201

Kennicutt, R.C. 1998, ARA&A 36, 189

Khochfar, S. & Burkert, A. 2006, A&A, 445, 403

Kitzbichler, M.G. & White, S.D.M. 2007

Kitzbichler, M.G. & White, S.D.M. 2008, MNRAS, 391, 1489

Le Févre, O., et al. 2000, MNRAS, 311, 565

Lilly, S.J., Le Févre, O., Hammer, F., & Crampton D. 1996, ApJ, 460, 1

Liske J., Lemon D.J., Driver S.P., Cross N.J.G., & Couch W.J. 2003, MNRAS, 344, 307

Lin, L. et al. 2004, ApJ, 617, L9

Lin, L. et al. 2008, ApJ, 681, 232

López-Sanjuan, C., Balcells M, Pérez-Gonzalez P.G., Barro G., Garca-Dabó C.E., Gallego J., & Zamorano J. 2009, A&A, 501, 505

Lotz, J.M., Primack, J., & Madau, P. 2004, AJ, 613, 262

López-Sanjuan, C., et al. 2011, A&A, in press; arXiv: 1009.5921v2

Lotz, J.M., et al 2008a, ApJ, 672, 177

Lotz, J.M., Jonsson,P., Cox, T.J., & Primack, J. 2008b, MNRAS, 391, 1137

Lotz, J.M., Jonsson,P., Cox, T.J., & Primack, J. 20010a, MNRAS,404, 575

Lotz, J.M., Jonsson,P., Cox, T.J., & Primack, J. 20010b, MNRAS,404, 590

Madau, P. , Ferguson, H.C., Dickinson, M.E., Giavalisco, M., Steidel, C.C., & Fruchter, A. 1996, MNRAS, 283, 1388

Masjedi, M., et al. 2006, ApJ, 644, 54

McGaugh, S.S., 2005, ApJ, 632, 859

Mihos, J. C. & Hernquist, L. 1996, ApJ, 464, 641

Moster, B.P., Somerville, R.S., Maulbetsch, C., van den Bosch, F.C., Macciò, A.V., Naab, T., & Oser, L. 2010, ApJ, 710, 903

Noeske, K., et al. 2007, ApJ, 660, L43

Panter, B., Jimenez, R., Heavens, A.F., & Charlot, S. 2007, MNRAS, 378, 378, 1550

Papovich, C., Finkelstein, S.L., Ferguson, H.C., Lotz, J.M., & Giavalisco, M. 2011, MNRAS, in press

Patton, D., et al. 2000, ApJ, 536, 153

Patton, D., et al. 2002, ApJ, 565, 208

Patton D.R., & Atfield J.E. 2008, ApJ, 685, 235

Pérez-González, P.G., et al. 2008, ApJ, 675, 234

Pozzeti, L., et al. 2007, A&A 474, 443

Rawat A., Hammer F., Kembhavi A.K., & Flores H., 2008, ApJ, 681, 1089

Rix, H., et al. 2004, ApJS, 152, 163

Robaina A.R., Bell E.F., van der Wel A., Somerville R.S., Skelton R.E., McIntosh D.H., Meisenheimer K., & Wolf C. 2010, ApJ, 719, 844

Rudnick, G., et al. 2003, ApJ, 599, 847

Salim, S., et al. 2007, ApJS, 173, 267

Salim, S., et al. 2009, ApJ, 700, 161

Sanders D.B., & Mirabel I.F. 1996, ARA&A, 34, 749

Scarlata, C., et al. 2007, ApJS, 172, 406

Scoville, N., et al. 2007, ApJS, 172, 1

Sheth, R.K. & Tormen, G. 1999, MNRAS, 308, 119

Shi, Y., Rieke, G., Lotz, J., & Pérez-González P.G. 2009, ApJ, 697, 1764

Somerville, R.S. & Kolatt, T.S. 1999, MNRAS, 305, 1

Somerville, R.S. , Primack, J.R., & Faber, S.M., 2001, MNRAS,320, 504

Somerville, R.S., Hopkins, P.F., Cox, T.J., Robertson, B.E., & Hernquist, L. 2008, MNRAS, 391, 481 [S08]

Springel, V., et al. 2005, Nature, 435, 629

Stewart, K.R., Bullock J.S., Wechsler R.H., Maller A.H., & Zentner A.R., ApJ, 2008, 683, 597

Stewart, K.R., Bullock, J.S., Barton, E.J., Wechsler, R.H. 2009a, ApJ, 702, 1005

Stewart, K.R., Bullock J.S., Wechsler R.H., & Maller A.H. 2009b, ApJ, 702, 307 [St09]

Stewart, K.R. 2009, in "Galaxy Evolution: Emerging Insights and Future Challenges", ASP Conference Series, Vol. 419, Edited by S. Jogee, I. Marinova, L. Hao, and G. A. Blanc. San Francisco: Astronomical Society of the Pacific, 2009., p.243

Tacconi, L.J. et al. 2010, Nature, 463, 781

Toomre, A. 1977, in Evolution of Galaxies and Stellar Populations, ed. B. M. Tinsley & R. B. Larson, (New Haven: Yale University Observatory), 401

van Dokkum, P. et al. 2010, ApJ, 709, 1018

Wetzel, A. R. 2010, MNRAS in press; arXiv:1001.4792W

Willmer, C.N.A., et al. 2006, ApJ, 647, 853

Wirth, G.D., et al. 2004, AJ, 127, 3121

White, S.D.M. & Rees, M.J. 1978, MNRAS, 183, 341

Yee, H.K.C. et al. 2000, ApJS, 129, 475

Zheng, Z., Coil, A.L., & Zehavi, I. 2007, ApJ, 667, 760